The Influence of Near-field Fluxes on Seasonal Carbon Dioxide Enhancements: Results From the Indianapolis Flux Experiment (INFLUX)

Natasha Miles, Kenneth Davis, Scott Richardson, Thomas Lauvaux, Douglas Martins, A.J. Deng, Nikolay Balashov, Kevin Gurney, Jianming Liang, Geoff Roest, et al.

The influence of near-field fluxes on seasonal carbon dioxide enhancements: Results from the Indianapolis Flux Experiment (INFLUX)

Natasha L. Miles[1], Kenneth J. Davis[1,2], Scott J. Richardson[1], Thomas Lauvaux[1,3], Douglas K. Martins[1,4], A.J. Deng[1,5], Nikolay Balashov[1,6], Kevin R. Gurney[7], Jianming Liang[7,8], Geoff Roest[7], Jonathan A. Wang[9,10], Jocelyn C. Turnbull[11,12]

[1]Department of Meteorology and Atmospheric Science, The Pennsylvania State University, University Park, Pennsylvania, 16802, USA
[2]Earth and Environmental Systems Institute, The Pennsylvania State University, University Park, Pennsylvania, 16802, USA
[3]Laboratoire des Sciences du Climat et de l'Environnement (LSCE), Saint-Aubin, 91190, France (current affiliation)
[4]FLIR Systems, Inc, West Lafayette, Indiana, 47906, USA (current affiliation)
[5]Utopus Insights, Inc., Valhalla, New York 10595 USA (current affiliation)
[6]NASA Goddard Space Flight Center/Universities Space Research Association, Greenbelt, Maryland, 20771, USA (current affiliation)
[7]Northern Arizona University, Flagstaff, AZ, 86011, USA
[8]Environmental Systems Research Institute, Redlands, California 92373, USA (current affiliation)
[9]Boston University, Boston, MA, 02215, USA
[10]University of California, Irvine, CA, 92697, USA (current affiliation)
[11]GNS Science, Lower Hutt 5040, New Zealand
[12]CIRES, University of Colorado at Boulder, CO, USA

Correspondence to: N. L. Miles (nmiles@psu.edu)

Abstract

Background
Networks of tower-based CO_2 mole fraction sensors have been deployed in and around cities across the world to quantify anthropogenic CO_2 emissions from metropolitan areas. A critical aspect in these approaches is the separation of atmospheric signatures from distant sources and sinks (i.e., the background) from local emissions and biogenic fluxes. We examined CO_2 enhancements compared to forested and agricultural background towers in Indianapolis, Indiana, USA, as a function of season and compared them to modeled results, as a part of the Indianapolis Flux (INFLUX) project.

Results
At the INFLUX urban tower sites, daytime growing season enhancement on a monthly timescale was up to 4.3 – 6.5 ppm, 2.6 times as large as those in the dormant season, on average. The enhancement differed significantly depending on choice of background and time of year, being 2.8 ppm higher in June and 1.8 ppm lower in August using a forested background tower compared to an agricultural background tower. A prediction based on land cover and observed CO_2 fluxes showed that differences in phenology and drawdown intensities drove measured differences in enhancements. Forward modelled CO_2 enhancements using fossil fuel and biogenic fluxes indicated growing season model-data mismatch of 1.1 ± 1.7 ppm for the agricultural background and 2.1 ± 0.5 ppm for the forested background, corresponding to 25 – 29 % of the modelled CO_2 enhancements. The model-data total CO_2 mismatch during the dormant season was low, – 0.1 ± 0.5 ppm.

Conclusions
Because growing season biogenic fluxes at the background towers are large, the urban enhancements must be disentangled from the biogenic signal, and growing season increases in CO_2 enhancement could be misinterpreted as increased anthropogenic fluxes if the background ecosystem CO_2 drawdown is not considered. The magnitude and timing of enhancements depend on the land cover type and net fluxes surrounding each background tower, so a simple box model is not appropriate for interpretation of these data. Quantification of the seasonality and magnitude of the biological fluxes in the study region using high-resolution and detailed biogenic models is necessary for the interpretation of tower-based urban CO_2 networks for cities with significant vegetation.

Keywords
Carbon dioxide, urban, greenhouse gas, fluxes, background, INFLUX, anthropogenic, biogenic

1 Background

The ability to accurately and expeditiously quantify urban greenhouse gas (GHG) emissions is essential for assessing the effectiveness of emission mitigation strategies. Each of numerous approaches to estimating urban CO_2 emissions has strengths and weaknesses, and the approaches are ideally used synergistically to improve each other (Davis et al. 2017). An advantage of in-situ tower- and building top- based atmospheric approaches is the ability to provide continuous quantification of emissions to support urban policy mitigation plans. Consequently, an increasing number of such GHG monitoring networks have been deployed in cities around the globe (e.g., McKain et al. 2012; Staufer et al. 2016; Boon et al. 2016; Miles et al. 2017a; Verhulst et al. 2017; Nickless et al. 2018).

The choice of background is critical for interpretation of data from urban CO_2 mole fraction networks because of the need to isolate the urban signal from variations associated with weather (Pal et al. 2020; Miles et al. 2012) and sources and sinks from other locations. The effect of background choices is an active area of research. Lauvaux et al. (2012) used two-step optimization of the boundary conditions, first utilizing aircraft and CarbonTracker mole fractions, and then optimizing within the inversion. McKain et al. (2012) used CO_2 mole fractions from a mountaintop site to represent the background CO_2, as did Lauvaux et al. (2013). Verhulst et al. (2017) analyzed four potential background sites for Los Angeles, California, and determined the annual average uncertainty in background using a local marine site to be roughly 10 % of the median mid-afternoon CO_2 enhancement for their 50-m AGL rooftop measurement site near downtown. For the CO_2-MEGAPARIS experiment, also described by Bréon et al. (2015) and Xueref-Remy et al. (2018), Staufer et al. (2016) used three CO_2 measurement sites in a Lagrangian configuration, with the background used depending on strictly defined wind speed and wind direction parameters. The site used as background for northeasterly winds was located in a small village considered a rural area, and the background site for southwesterly winds was near the southwest corner of Paris, in a mixed urban and rural area. Sargent et al. (2018) calculated a curtain of background values using data from two background sites 90 – 170 km from Boston, MA, combined with modelled vertical mole fraction gradients, and limited the analysis to days with wind directions within ±40° of the background to urban site vector. CO_2 for each edge of the model domain boundaries was determined by Nickless et al. (2018) using a Global Atmosphere Watch (GAW) station located 60 km to the south of Cape Town, South Africa. The determination of background for Cape Town was aided by its location on a peninsula. Mueller et al. (2018) used modeling and geostatistical methods with synthetic data to determine optimal locations for four background towers in the Washington D.C./Baltimore area. Cities predominately downwind of large bodies of water or located in non-vegetated regions are simpler in terms of determination of background, but most cities, including those described above, are near other cities and/or surrounded by active vegetation, complicating the extraction of local signals.

The Indianapolis Flux Project (INFLUX) is a testbed for measuring urban GHG emissions in Indianapolis, Indiana (Davis et al. 2017; Whetstone, 2018). For the dormant season in Indianapolis, roughly November – March, the biogenic effect on CO_2 fluxes is relatively small compared to the fossil fuel contribution. Turnbull et al. (2015a) found that wintertime total CO_2 in Indianapolis was nearly equivalent to the fossil-fuel only CO_2 using a local background. Also in Indianapolis, Miles et al. (2017a) used a single predominantly upwind tower site 20 km to the southwest of the city edge as background for an analysis of inter-tower differences during the dormant season 2012 – 2013. Lauvaux et al. (2016) found that inverse emission results differed by only 4 % between using a single background and using a wind direction dependent background, for their primarily dormant season analysis of data between September 2012 – April 2013. Turnbull et al. (2019) used flask measurements of $^{14}CO_2$ to determine that biogenic CO_2 fluxes in Indianapolis are just10 % of the magnitude of fossil fuel CO_2 fluxes in November and December.

For analyses encompassing the growing season, and for cities without dormant seasons, however, biogenic contributions to the total flux are potentially substantial and must be addressed (Nickless et al. 2018). In the growing season, biological fluxes significantly impact the determination of the urban carbon budget (Wu et al. 2018; Kornei, 2018; Turnbull et al, 2015a). In addition to a strong seasonal cycle in biological CO_2 fluxes, different vegetation types are known to exhibit different timing of fluxes. For example, crops have shorter growing seasons and more intense carbon drawdown than natural vegetation (Gervois et al. 2004; Lokupitiya et al. 2009). Corbin et al. (2010) found that simulating corn and soybean explicitly alters both the timing and magnitude of the net carbon fluxes compared to generic agriculture/ grassland. Increasing agricultural land use and yields between 1961 and 2010 manifested in a 15 % long-term increase in CO_2 seasonal amplitude and a shift in overall vegetation growth by

one to two weeks (Zeng et al. 2014). Differences in green-up dates of local vegetation were correlated with associated patterns in CO_2 in Boston (Briber et al. 2013). In the U.S. Upper Midwest, Miles et al. (2012) found large growing season mean differences in CO_2 (5.1 ppm) between a tower site dominated by corn versus one dominated by grass. Comparatively, a downtown tower in Indianapolis measured 2.9 ppm higher than a forested tower during the dormant season. Thus biological fluxes can be on the same order of magnitude as anthropogenic fluxes and need to be taken into account when interpreting urban CO_2 observations.

Evaluation of the impact of background biological fluxes on urban CO_2 flux estimates has, to date, relied heavily upon simulations of these fluxes. Nickless et al. (2018) used the Community Atmosphere Biosphere Land Exchange (CABLE) model to represent biogenic fluxes for their inversion of CO_2 fluxes in Cape Town, South Africa. While the inversion was able to improve the total flux estimates, it was not able to disaggregate the biogenic from anthropogenic fluxes because of the large uncertainties in the biogenic flux priors. Sargent et al. (2018) used the UrbanVPRM and a biomass map to simulate the impact of rural biology on background CO_2 for the city of Boston. Heimburger et al. (2017) and other aircraft studies show that background CO_2 mole fractions often exhibit complex spatial structure. Balashov et al. (2019) show that Indianapolis CH_4 backgrounds vary in space with large random and systematic differences across background sites, likely attributable to large plumes from coal mines in southwest Indiana. Direct evaluation of background CO_2 via long-term observation is needed to assess the accuracy of our urban inversion systems.

The goal of this paper is to document the effects of background choice on CO_2 enhancements measured with an urban tower-based network, and compare them to the overall enhancements. We first consider the differences between background towers as a function of wind direction and season. Two potential background towers were available for January 2013 – December 2018, and an additional one was available for April 2017 – December 2018. We calculated 31-day median afternoon enhancements above each of the primary background towers, and composited over 5.7 years of data to determine yearly cycles of enhancements at each tower. We compared the results from each of the background towers, and made a simple prediction to explain the difference between the towers based on their land cover types. We then compare these results to forward model CO_2 enhancement using fossil fuel and biogenic fluxes.

2 Methods

2.1 Study site

The locations of the INFLUX ground-based CO_2 measurement sites and the city of Indianapolis, Indiana, in the U.S. Midwest, are shown in Fig. 1. Indianapolis, in Marion County, Indiana, was the 17th most populous city in the U.S. in 2019, with an estimated population of about 876,000 (US Census, 2020). The predominant wind direction in Indianapolis is from the southwest, with southerly through westerly winds occurring 37.7 % of the times with appreciable wind speed throughout 2018 (Desert Research Institute, 2019). Three of the INFLUX tower sites are considered potential background sites: Towers 01, 09, and 14. Tower 01 is upwind of the edge of the city (as defined by the beltway encircling the city) by 20 km when the wind is from the predominant southwesterly direction, and is on the northern edge of a forested area (Fig. 1). Tower 09 is located in an agricultural area 24 km east of the edge of Indianapolis. Tower 14 was installed in late April 2017, and is northwest of the city by 50 km, again in a primarily agricultural region. The remaining tower sites are in and around Indianapolis (Miles et al. 2017a).

The primary biogenic land cover types in the region surrounding Indianapolis (Fig. 1) are forest, agricultural (including corn and soy), and grassland/pasture, and the biological fluxes from these land cover types differ significantly in their seasonal cycles (Fig. 2a). The forest fluxes shown in Fig. 2a were measured at a flux tower (Kim et al. 2015) in the Morgan Monroe State Forest (MMSF), 29 km to the south of Tower 01. The monthly average flux is negative in the growing season (i.e., CO_2 drawdown) beginning in May and extending through September. The forest flux was weakly positive throughout the remainder of the year. A corn/soy flux tower (Hollinger et al. 2005) was located in Bondville, Illinois, 176 km WNW of Tower 01. Corn and soy were grown in the field surrounding the flux tower in alternating years. The growing season, as indicated by negative fluxes, for corn begins later than for the forest, in June and extended through August. The soy flux was negative only for the months of July and August. As for the forest, the agricultural fluxes were weakly positive during the dormant

season. Grassland/pasture tends to be on the edges of other landcover types in small patches (Miles et al. (2017, Fig. 1).

The domain-averaged fossil fuel CO_2 flux (Hestia, Fig. 2b) exhibited higher values in the colder months of November – March, due to energy production for heating (e.g., Gurney et al. 2012; Lauvaux et al. 2013; Staufer et al. 2016). The summer increase in fossil fuel emissions was likely attributable to energy production for cooling (Blasing et al. 2005; Ueyama and Ando, 2016).

2.2 Instrumentation

The INFLUX in-situ observation network includes tower sites measuring greenhouse gases using wavelength-scanned cavity ring down spectroscopic (CRDS) instruments (Picarro, Inc., models G1301, G2301, G2302, and G2401). The full network consists of twelve sites but with site re-locations throughout the period, there are a total of fourteen measurement locations. We focus on CO_2 measured during the period January 2013 – December 2018 for this paper. The instruments were deployed at the base of existing communications towers, with ¼" (0.64 cm) sampling tubes installed as high as possible on each tower (39 – 136 above ground level (AGL)). Four of the towers had multiple measurement heights (Table 1).

A linear calibration based on three to five NOAA tertiary reference tanks was applied to the instruments prior to deployment and following any manufacturer repairs, and an intercept-only calibration was applied in the field every 23 hours based on one or two calibrated reference tanks. For the majority of the time period, the air samples were dried using Nafion dryers (MD-070-96S-2, PermaPure) in reflux mode, with an internal water vapor correction applied for the effects of the remaining water vapor (< 0.2 or 0.6 %, depending on the length of the Nafion dryer). We used hourly means of CO_2, which were reported on the WMO X2007 scale and are publicly available (Miles et al. 2017b). Compatibility of the INFLUX network, both within network and compared to the global network, was assessed via co-located NOAA flask systems (Turnbull et al. 2012) at Towers 01, 02, 03, 06, 09, and 10, and round-robin type testing using multiple NOAA-calibrated tanks, indicating compatibility of 0.18 ppm CO_2. Further details of the instrumentation and compatibility are described by Richardson et al. (2017) and Miles et al. (2017a).

Because of unexpectedly low CO_2 mole fractions measured at Tower 14 during the growing season of 2017, a separate instrument with a separate ¼" (0.64 cm) tube installed to the top of the tower was co-located at the site for a period of several weeks to eliminate the possibility of further leaks or other instrument problems. The additional instrument was calibrated prior to deployment and installed with no drying, relying on the internal water vapor correction for CO_2. From 20 – 26 August 2018, both instruments sampled from the top of the tower and the difference between the two (primary instrument – secondary instrument) was very small, –0.11± 0.12 ppm.

2.3 Wind measurements

The wind data used to characterize overall synoptic patterns in the city were measured at the Indianapolis International Airport, outside the southwest corner of the city. The data are part of the Integrated Surface Dataset (https://www.ncdc.noaa.gov/isd). The weather station at the airport uses the Automated Surface Observing System (http://www.nws.noaa.gov/asos/pdfs/aum-toc.pdf). The accuracy of wind speed is ±1.0 ms^{-1} or 5 % (whichever is greater) and the accuracy of wind direction is 5° when the wind speed is ≥ 2.6 ms^{-1}. Wind directions are not reported for periods in which the wind speed is less than 1.6 ms^{-1}. The height of the wind instrument is about 10 m AGL. The wind data are reported at a single point in time recorded within the last 10 minutes of each hour.
For the purpose of categorizing afternoon-average CO_2 in terms of wind direction, we calculated vector averages of afternoon winds.

2.4 Determination of land cover surrounding tower locations

In order to characterize each of the INFLUX tower locations in terms of the surrounding land cover types, we considered the land cover within 10 km of each tower. This radius covers approximately 80 % of the influence for

the towers, determined via afternoon influence functions simulated for January – April 2013 at 1-km resolution with the Lagrangian Particle Dispersion Model (LDPM) (Uliasz, 1994; Lauvaux et al. 2016), using inputs from the Weather Research Forecasting - Four-Dimensional Data Assimilation modeling system (WRF-FDDA-CO_2) (Stauffer and Seaman 1994; Deng et al. 2004; Deng et al. 2009).

Land cover data was obtained from the United States Department of Agriculture National Agriculture Statistics Service (NASS; https://nassgeodata.gmu.edu/CropScape/ Han et al. 2014). The categories with significant percentages in the Indianapolis area included corn, soy, open water, developed/open space, developed/low intensity, developed/medium intensity, developed/high intensity, deciduous forest, and grass/pasture. The most recent year available from NASS, 2018, was used for the analysis. Corn and soy are typically rotated each year, but since we are considering a large area, a single year is a reasonable representation of the overall landcover for the time period.

We defined the total urban fraction for each tower as the fraction of area categorized as "developed", compared to the total area within a 10-km radius (80% of the footprint) of each the towers. We then ranked the towers in terms of total urban fraction. Each category of "developed" (i.e., open, low-, medium- and high-intensity) was weighted equally for this purpose, given that the proportions of these categories do not differ considerably between the INFLUX sites.

The prevalence of different land cover types differed considerably between the INFLUX towers. The percentages of land cover types within each category surrounding each tower are shown in Fig. 3. The towers with the highest urban fractions within the surrounding area were Tower 03 (94.5 %), Tower 11 (91.4 %), Tower 10 (89.4 %), Tower 07 (80.7 %), Tower 05 (80.6 %), Tower 12 (77.2 %), Tower 02 (74.0 %), and Tower 06 (70.6 %). We consider these "urban" towers. The remaining towers were surrounded by 48 % or less urban fraction and are considered "rural" towers. The potential background towers, Towers 09, 01 and 14 were surrounded by 12.3 %, 12.3 % and 6.2 % urban land cover, respectively. Tower 01 was surrounded by the highest fraction of deciduous forest (35.1 %). Towers 14 and 09 were primarily agricultural sites (covering 78.5 and 70.7 %, respectively, of the surrounding areas). Tower 14 had the highest percentage of corn (36.4 %), with Towers 09 at 30.4 %. Soy is the other major crop in the region.

2.5 Observational Analyses

In this paper, we focused on afternoon average CO_2, with the mean calculated over the period 1700–2200 UTC (1200–1700 LST). The atmospheric boundary layer (ABL) is typically well mixed during these hours, which allows simpler interpretation of the measurements (e.g., Bakwin et al. 1998).

We considered three towers as potential background sites in this paper. Miles et al. (2017a) used Tower 01 (forested) as the background tower for the INFLUX network during the dormant season, and determined the enhancement in CO_2 of the other towers compared to it. Here we considered Towers 09 and 14 (both agricultural) as additional background towers. Both Towers 01 and 09 data were available for the majority of the analysis period, January 2013 – December 2018, but Tower 14 was only available from April 2017 through December 2018.

We compared the CO_2 measured at the INFLUX sites by calculating the 31-day running median of the enhancement in CO_2 for each of the towers from Tower 01 and from Tower 09. Here we use the term enhancement although the difference can be negative, and we note that we have not isolated the anthropogenic enhancement with this calculation. We excluded data points for which any of the background towers were downwind of the urban area (afternoon average wind directions of 20 – 65° (Tower 01 in urban plume) and 235 – 280° (Tower 09 in urban plume). To determine these wind directions, we considered the angle between the background towers and the geometric edges of the urban area, as defined as the region within the expressway encircling Indianapolis (I-465) and the differences between background towers as a function of wind direction in the dormant season. The urban plume was not apparent at Tower 14. Furthermore, median results centered within 10 days of extended data gaps attributable to instrument malfunctions were excluded. We averaged these results for each day of the year for the available years between January 2013 and December 2018 to form annual cycles of smoothed composited CO_2 differences. The standard deviation of the data from each of the available years was used as an estimate of the variability. We compared the results using Tower 09 as a background to those using Tower 01 as a background. The enhancements at each tower using these two different backgrounds can be compared since the same wind directions were excluded from each. We have primarily approached the background in an Eulerian sense,

comparing each tower's measurements to a background at the same point in time, afternoon averages for this case. We also considered a more Lagrangian approach, utilizing a wind-direction dependent background, with Tower 01 as a background for wind directions from the west (180 – 360°) and Tower 09 as a background for wind directions from the east (0 – 180°), as done by Lauvaux et al. (2016).

Assuming no missing data, the difference in each tower (Tower N) enhancement using Tower 01 as a background ($CO_{2,Tower\ N} - CO_{2,Tower\ 01}$) and those using Tower 09 as a background ($CO_{2,Tower\ N} - CO_{2,Tower\ 09}$) is equivalent to subtracting Tower 09 from Tower 01, since $CO_{2,Tower\ N}$ cancels out. To compare the differences caused by background choice to the enhancement, we normalized the difference in enhancement between using two different background towers by the enhancement using Tower 01 as background and determined the percent difference.

We hypothesize that the differences between Tower 09 and Tower 01 (and thus between the enhancements using these two towers as background) to be attributable to differences in the primary land cover types and corresponding fluxes surrounding these towers. For a measurement site with a finite number of landcover types (lc) in the surrounding region, the CO_2 measured is related to the mean flux from each landcover type (F_{lc}) and the fractional area of that landcover type (f_{lc}),

$$CO_2 = a \sum_{lc=1}^{N} F_{lc} f_{lc,} \quad (1)$$

where a is a constant. The landcover surrounding Towers 09 and 01 is predominately agricultural and forest, with Tower 09 having a higher percentage of agricultural landcover (71%) and Tower 01 having a higher percentage of forest landcover (35%) and a smaller portion of agricultural landcover (34%). Following from Eq. (1), we assert that,

$$\Delta CO_2 / a = (F_{forest} f_{forest,01} + F_{agr} f_{agr,01}) - (F_{forest} f_{forest,09} + F_{ag} f_{agr,09}), \quad (2)$$

where ΔCO_2 is the difference in CO_2 mole fraction between the two tower sites, F_{forest} and F_{agr} are the forest and the mean of the corn and soy agricultural fluxes, and f_{forest} and f_{agr} are the forest and agricultural land cover fractions for the area of 10 km radius surrounding each site. We note that corn and soy are typically rotated from year to year and have similar areal coverage within the region. For these reasons, although corn and soy have very different fluxes, we simplified the calculation by averaging the corn and soy fluxes to determine an agricultural flux.

This equation is based on the scale conservation equation, and assumes that all factors other than the surface fluxes are equivalent at the two tower locations. We used the forest, corn and soy fluxes shown in Fig. 2a to represent the seasonal pattern of ecosystem flux and predicted midday ABL CO_2 mole fraction differences between these two background sites. We then compared the seasonal pattern of the predicted CO_2 difference to the measured differences at Tower 01 and 09.

2.6 Modelled Tower CO_2

We calculated forward modelled CO_2 dry mole fractions at each of the INFLUX towers by convolving tower footprints, representing the relationship between mole fractions and surface fluxes with fossil fuel emissions and biogenic fluxes. The tower footprints were simulated using transport field derived from the Weather Research and Forecasting model (WRFv3.6.1, Skamarock and Klemp, 2008) in Four-Dimensional Data Assimilation mode for the inner 1-km resolution 87 km x 87 km domain (Deng et al. 2017). Data from World Meteorological Organization surface stations within the model domain were assimilated to nudge the model to the observations. The transport fields were then coupled offline to the Lagrangian Particle Dispersion Model (Uliasz 1994; Lauvaux et al. 2012; Lauvaux et al. 2020) in backward mode.

Fossil fuel emissions from the Hestia CO_2 emissions inventory product (Gurney et al. 2017; Gurney et al. 2019), available for each of eight economic sectors (residential, on-road mobile, off-road mobile, industrial, commercial, electricity production, airport, and railroad) were used. Hestia emissions were aggregated from the initial building-level product to 1-km resolution, covering Marion County and the eight surrounding counties.

For biogenic fluxes, we used the urban Vegetation Photosynthesis and Respiration Model (VPRM, Mahadevan et al. 2008; Hardiman et al. 2017), driven by greenness data from the Moderate Resolution Imaging Spectroradiometer (MODIS) satellite product and climate data from the North America Regional Reanalysis (NARR). The fraction of impervious surface area from the National Land Cover Database (Han et al. 2014) within each pixel was used to adjust the carbon fluxes for the impact of urbanization on ecosystem function. Non-paved portions of the city were defined as deciduous broadleaf forest. Distributions for four land cover types (corn, soy, grassland/pasture, and forest) were derived from the United States Department of Agriculture National Agriculture Statistics Service (NASS; https://nassgeodata.gmu.edu/CropScape/, Han et al. 2014), and the VPRM parameters were optimized for these land cover types (Hilton et al. 2014) to produce hourly carbon fluxes at 1-km resolution as the weighted average of carbon fluxes from each type. Note that Tower 14 is outside the domain of the VPRM results and is thus not included in the model-data mismatch analysis.

We then compared the 31-day running median forward modelled CO_2 enhancements for 2014 to observed CO_2 enhancements for the same year. We used 1200 – 1700 LST, with the footprints incorporating fluxes in the 4 hours preceding the observations. Wind directions for which either Tower 01 or Tower 09 were within the urban plume were excluded in both the model results and the observations. We then calculated urban site (Towers 02, 03, 06, 07, and 10) averaged model-data mismatch as a function of month of year. Although the percentage of urban landcover surrounding Tower 11 was quite high, we did not include it in the urban site calculations because the forward modelled anthropogenic CO_2 at Tower 11 was very low.

3 Results

3.1 CO_2 enhancements above background

3.1.1 Observed CO_2 enhancements

When comparing CO_2 measured at INFLUX towers to a background tower over an annual timescale, biogenic effects were a dominant feature. The smoothed composited midday ABL CO_2 mole fraction enhancements relative to Tower 09 (agricultural) are shown in Fig. 4. The overall pattern, consistent for most of the towers, was a maximum in August, a secondary maximum in December – January, and minima in June and October. While anthropogenic fossil fuel CO_2 emissions have a seasonal pattern (Fig. 2), the intensity of the growing season enhancements is attributable to biogenic effects primarily at the background tower, as will be described.

Not surprisingly, the towers with highest urban fraction in the surrounding area as shown in Fig. 3 exhibited generally higher smoothed composited CO_2 enhancements relative to agricultural Tower 09 (Fig. 4). There was a clear demarcation between the 'urban' towers, those with greater than 70 % surrounding urban land cover (Towers 03, 11, 02, 10, 07, and 06), and the 'rural' towers with 48 % or less urban fraction (Towers 08, 04, 13, 01, and 14). The dominant feature of this figure, the maxima in July/August, was likely attributable to the reduced agricultural and forested land cover within the footprints of the urban towers and thus reduced biogenic uptake of CO_2 compared to the background tower. In the dormant season, the higher urban tower enhancements were likely due to larger anthropogenic fluxes than for the rural sites. The August enhancements for the urban towers averaged 4.2 ppm, 2.6 times as large as the February urban tower enhancements, which averaged 1.6 ppm. The rural Towers 08, 04, 13, and 01 also exhibited peak growing season maxima compared to Tower 09 but in the range of 1.0 – 2.5 ppm rather than 4.3 – 6.5 ppm for the urban towers. The notable difference between Tower 14 and Tower 09 (both agricultural) is discussed in Section 3.1.5.

3.1.2 Sensitivity of urban CO_2 enhancement to the choice of background

The INFLUX urban tower-average observed enhancements (Towers 02, 03, 06, 07, and 10) were sensitive to the choice of background tower (Fig. 5) during the growing season. While the overall pattern of enhancements (i.e., large summertime enhancement) was evident when comparing to either forested Tower 01 or agricultural Tower 09, the timing of the initiation of the growing season peak differed. The difference in enhancements using the different

background towers was significantly larger, however, between May and September, and it switched sign at the beginning of July. In June the difference between using Tower 01 as a background and using Tower 09 as a background was –2.8 ppm and in August the difference was 1.8 ppm. For the dormant season, the difference in enhancement incurred by using different backgrounds was relatively small, 0.4 ppm on average.

We postulate that the differences between the enhancements using these two background towers is attributable primarily to the rural biogenic signal, and assume no significant seasonal cycle in the urban biology. Shown in Fig. 6a is the difference between these two background towers, composited over 2013 – 2018 and for the year for which modelled results are available (2014). The growing season differences between the two towers were stronger in August – September 2014, outside of one standard deviation from the mean of the years, but not as pronounced for May - June. The predicted seasonal pattern CO_2 difference between Tower 09 and Tower 01, based on forest and agricultural fluxes (Fig. 2a) are shown in Fig. 6b. The prediction, based on Eq. 2, is dimensionless and the focus is on relative trends of the differences (i.e., the shape of the curve). As in the composited observations for 2013 – 2018 (Fig. 6a), the predicted pattern was low from January through April. In May, Tower 01 CO_2 was predicted to be its greatest magnitude lower than Tower 09 CO_2. This is attributable to forest drawdown in the area surrounding Tower 01. Leaf-out usually occurs in the Morgan-Monroe Forest south of Tower 01 beginning at the end of April and is 80 % complete by the month of May (Kim et al. 2015), compared to agricultural drawdown which begins later in the year, June for corn and July for soybean (Fig. 2a). This conclusion is consistent with large enhancements noted when the wind was from the south in Fig. S3c. The predicted pattern in background tower differences (Fig. 6b) was similar to the observed minimum (Fig. 6a) in June, but slightly ahead in time. The Tower 09 CO_2 was predicted to be its greatest magnitude lower than Tower 01 in mid-July, only a two-week shift from the observed pattern. That is, by mid-July, the agricultural fluxes in the footprint of Tower 09 were maximally larger than the forest fluxes in the footprint of Tower 01. While the predicted CO_2 difference was small in November and December, as observed, the prediction indicated an additional minimum in September (about one half the magnitude of the minimum in May) that was not observed in the tower data. According to the fluxes in Fig. 2a, the forest was expected to continue to draw down CO_2 in September, whereas the agricultural fluxes indicated small magnitude respiration. The tower results, however, indicated the both forest and agricultural fluxes were roughly balanced by mid-September, averaged over the time period of the dataset.

The forward model using VPRM and Hestia fluxes predicts an observed negative difference between Towers 09 and 01 in May and June and was largely consistent with observed differences throughout the rest of the year, but missed the positive difference in August and September (Fig. 6c). For May – mid June, the differences were –1.0 ppm, Then, as for the prediction based on simple fluxes and landcover types, the mismatch switches sign and averages +0.9 ppm for mid June – mid July. In the later part of the summer, August through mid September, the model predicts the towers to have nearly the same CO_2, missing the +3.0 ppm observed difference. Improvements in the biogenic model can minimize these differences. Additionally an inversion using CO_2 and CO mole fractions can optimize both the fossil and the biogenic CO_2 separately (Lauvaux et al. 2020).

3.1.3 Differential footprints

A box model assumes that the species of interest measured downwind is that measured at an upwind location, changed only by the fluxes from the surface below the box. This approach is not appropriate for interpretation of the application described here because the influence function for each tower decreases exponentially with distance from the towers (Uliasz et al. 1994) and thus the tower footprints do not overlap to a large degree. Here we have considered one background regardless of wind direction in an Eulerian framework (ignoring wind direction for which either background tower was within the urban plume), but biological fluxes must be considered for more Lagrangian approaches (following an air parcel from a background tower to an urban tower) as well. Using a wind-direction-dependent background while still excluding urban plumes for the background towers yielded similar results in terms of predominant growing season enhancement not likely to be attributable to changing anthropogenic emissions (Fig. S4c). Contributions to the CO_2 measured at a tower decrease exponentially with distance (e.g., Uliasz et al. 1994). The footprints for a background and an urban tower overlap, but each tower is influenced preferentially by nearby sources, and we call this the differential footprint. If we consider a contour containing a given percentage of the influence, we can visualize the differing effect of the rural biological flux as in Fig. 7.

3.1.4 Modelled urban-tower averaged CO_2 enhancements

The forward model predicted a growing season increase in enhancement in CO_2 at the tower sites (Fig. 8a). Furthermore, the model was able to capture the observed timing difference in green-up between using forested Tower 01 and agricultural Tower 09 as backgrounds, in general. However, modelled enhancements were larger than observed (Fig. 5) during the growing season. The modelled difference between the CO_2 of the background towers was similar to that observed in June (2.9 ppm modelled, compared to the observed 2.5 ppm), but in August, the model predicted the forested background tower CO_2 to be lower than the agricultural tower by 1.7 ppm, whereas the observations showed the agricultural tower CO_2 to be lower by 2.0 ppm.)

The INFLUX urban tower-averaged (Towers 02, 03, 06, 07, and 10) model-data mismatch, resulting from a combination of differences attributable to fossil fuel fluxes, biogenic fluxes and transport, was larger during the growing season (May – September) compared to the dormant season (Fig. 8b). For the dormant season, the mean model-data mismatch was -0.1 ± 0.5 ppm. The mean growing season model-data mismatch was 1.1 ± 1.7 ppm for enhancements compared to Tower 09 (agricultural) and 2.1 ± 0.5 ppm for those compared to Tower 01 (forested), with the standard deviations calculated over the months. The modelled enhancements were positive in the growing season, likely indicating stronger modeled drawdown at the background sites than was observed, with the mismatch being higher for the forested background site. The INFLUX tower-averaged model-data mismatch averaged 25 % of the modelled CO_2 enhancement for Tower 09 and 29% for Tower 01 during the growing season.

3.1.5 Agricultural tower CO_2 background differences

The median daytime CO_2 at Towers 14 and 09 differed by up to 2.5 ppm in the peak growing season, despite both being agricultural sites (Fig. 9). Tower 14, in west-central Indiana is on the eastern edge of the highly productive U.S. corn belt (Fig. S5). Tower 14 is located in Montgomery County, which produced 1.35×10^6 kg corn / harvested km^2, whereas Hancock County (Tower 09) produced 1.06×10^6 kg corn / harvested km^2 (USDA NASS 2018). In addition, the area surrounding Tower 14 contains 37.1 % corn landcover (Section 3.1), whereas the area surrounding Tower 09 is 33.8 % corn. Thus the combination of a higher percentage of corn coverage and more productive harvests is likely to have contributed to the additional CO_2 drawdown observed at Tower 14 compared to Tower 09.

We explored other potential causes, but none seem likely to explain the large observed differences between these two towers. Measurement height does likely contribute, but not enough to explain the difference (see also Section S4). The measurement heights of the three potential background towers (Towers 01, 09, and 14) are 121, 130, and 76 m AGL, respectively. Linearly interpolating the mean CO_2 difference found between tower heights in the growing season at Tower 01 (Fig. S6), the magnitude of the difference between 76 m AGL and 121 m AGL was 0.3 ppm. This analysis is an overly conservative estimate since vertical CO_2 gradients are non-linear (Wang et al. 2007). Typical corn fluxes in July and August are about double those of forest (Fig. 2a), so the height effect difference between Tower 14 and Tower 09 is estimated to be no more than 0.6 ppm.

Although we ignored wind directions for which the primary plume from Indianapolis affected the background towers, there are still small urban areas within the footprints of the towers. The urban fraction within the 10-km^2 area contributing about 80 % of the influence on the CO_2 measurements at Tower 09 was 12.3 %, compared to 6.2 % surrounding Tower 14. Thus increased anthropogenic signal at Tower 09 may have somewhat reduced the apparent biological signal, increasing the difference between Tower 14 and Tower 09. Tower 14 is outside the modeling domain, and thus has not been considered extensively in this work.

4 Discussion/Conclusions

We examined CO_2 enhancements as a function of time throughout the year using composites of over five years of data from towers in and around the city of Indianapolis, IN. Three possible background towers were considered, Tower 01 in a forested area southwest of the city, Tower 09 in an agricultural region east of the city, and Tower 14 in an agricultural region northwest of the city. The enhancement differed significantly depending on choice of

background and time of year, being 2.8 ppm higher in June and 1.8 ppm lower in August using Tower 01 as a background compared to Tower 09.

The most striking feature in the CO_2 enhancements compared to agricultural Tower 09 as a background was an apparent maximum in August, with 31-day median enhancement at the urban towers up to 4.3 – 6.5 ppm, 2.6 times as large as those in the dormant season. This feature could be misinterpreted solely as an anthropogenic signal, but the cause was a combination of the effect of the biological signal upwind of the background tower, and a secondary maximum in the fossil fuel flux (Fig. 2b). Clearly the biological fluxes (and land cover types) upwind of the background measurement sites must be known in order to interpret CO_2 enhancements throughout the year. Anthropogenic fluxes resulting from an inverse estimation which did not consider biological fluxes in the rural areas around the city would overestimate the summertime anthropogenic fluxes. We note that using a model-data hybrid approach for determination of background (Sargent et al. 2018) minimizes the effect of the biogenic signal in the calculated enhancements. Our approach, using a measured background, means that the enhancements are quite dependent on the biogenic signal of the background towers, and the enhancements are not "anthropogenic" enhancements. In the next step, optimization of fluxes using an inversion (Lauvaux et al. 2020), the biogenic portion is determined via either method of background determination.

The difference in timing of fluxes from the different land cover types of the background towers appears to explain the shift in summertime peak for the urban towers from August when using agricultural Tower 09 as a background to July when using forested Tower 01 as a background.

While the differences in the growing season enhancements using different backgrounds was sizeable, a prediction of the difference between Tower 09 and Tower 01 CO_2 based on differences in land cover type in the surrounding areas and the typical fluxes of these land cover types yielded a plausible explanation, with the difference attributable to the forest green-up preceding that of agriculture, but the agricultural peak drawdown being more intense. Forward modelled total CO_2 using Hestia fossil fuel emissions and VPRM biogenic fluxes show that the biogenic model was able to represent the enhancements fairly well, with model-data mismatch of 1.1 ± 1.7 ppm for the agricultural background and 2.1 ± 0.5 ppm for the forested background during the growing season (25 – 29 % of the modelled CO_2 enhancement) and -0.1 ± 0.5 ppm during the dormant season. Developing and testing robust CO_2 flux estimates for the rural ecosystems upwind of cities is therefore critical to year-round urban anthropogenic CO_2 flux estimates. Further tuning of the biogenic model response, or a more advanced vegetation model in order to more fully capture the timing and productivity differences between the forested and agricultural sites considered here would likely improve the inversion results. The sensitivity of the inverse fluxes to the biogenic fluxes is of course dependent upon the fossil fuel emissions for the study area.

The growing season model-data mismatch was larger than the dormant season mismatch, suggesting that biogenic fluxes were a larger source of mismatch than the fossil fuel fluxes. Unfortunately, we were not able to use the flask measurements to decompose into biogenic and fossil fuel components of the mismatch because 1) the flasks were sampled when the winds were from the west/southwest, i.e., to a large extent, the wind directions ignored for this analysis, and 2) differing subset of towers for this analysis vs the flask availability. However, the inversion of these data, separately optimizing fossil fuel and biogenic CO_2 emissions, (Lauvaux et al. 2020) indicated very little adjustment to the fossil fuel CO_2 emissions from Hestia, further corroborating that the biogenic model is a larger contributor to the model-data mismatch.

The summertime increase in enhancement was larger in forward model results than is observed, indicating that the VPRM fluxes were in general too strong, or that the modelled biosphere was too weak within the urban domain. Further analysis will assess the performance of VPRM via flux towers and tune the biogenic model to improve accuracy. Accurate modelling of ecosystems will be crucial for accurate fluxes during the growing season, for both the approach presented here, based on a simple background tower or wind-direction dependent tower, and the model-data hybrid approach for background determination (Sargent et al. 2018). Another approach is to optimize the biogenic fluxes separately in the inversion (Lauvaux et al. 2012).

Enhanced intensity of drawdown due to corn during the peak growing season months of July and August northwest of Indianapolis was the likely cause of the large difference in CO_2 measured at Towers 09 and 14, both in agricultural areas. The discrepancy between background agricultural sites during the peak growing season months was similar in magnitude to the differences between urban towers and Tower 01. Tower 14 is on the predominately

downwind edge of the U.S. corn belt, and while there is corn grown in the area surrounding Tower 09 it is a less productive area overall. Persistent differences in CO_2 between two background sites with similar land cover presents an additional challenge for vegetation models. The biogenic model may need to be further tuned to capture the differences between these agricultural sites with differing productivity. INFLUX is unique being on the edge of the U.S. corn belt, but in general, potential gradients in production and differing landcover type within domains for each study should be considered. Additional measurements, including flux tower eddy covariances are planned to learn more about the differences in CO_2 drawdown between these locations.

Although the number of towers and timespan of the dataset is unprecedented for a study of CO_2 mole fractions in and around a city, there were some limitations of this study. We used afternoon-averaged wind direction at the airport to exclude the afternoons for which the background towers were affected by the urban plume. Given the likelihood of wind direction changes throughout the day, back trajectory analysis would have been a more accurate way to exclude the urban plume, but is beyond the scope of this study. Additionally, although we estimated the effects of variable tower heights on our results and found them to be negligible (Fig. S7), ideally all measurements would be made at the same height. In practice, this was not possible. Furthermore, we used a 10-km radius to categorize land cover types for each tower for the simple calculation shown in Fig. 5c. In reality, the area affecting the CO_2 measured at each tower is much more complex and we did not address the seasonal cycle of the urban biosphere for the simple calculation. We have addressed these issues to a degree by comparing the observed enhancements to the forward modelled CO_2. The modelled footprints were calculated on the inner, 1-km resolution, 87 km x 87 km domain, and likely extended beyond this domain. Future analysis will include footprints calculated on a larger domain.

This study in general highlights the importance of background choice in urban greenhouse gas studies. The magnitude of potential background differences depends on time of year and land cover types in the region. Indianapolis is a large city, but not a mega city, and determination of fluxes for larger cities with larger CO_2 fluxes may be less affected by land cover-based differences in background towers. Still, careful consideration of land cover types is necessary in order to interpret CO_2 tower network data throughout the growing season. Each city, depending on topography, climate, population, surrounding land cover and other factors, has unique challenges for the estimation of greenhouse gas emissions.

Declarations

Availability of data

Miles NL, Richardson SJ, Davis KJ, Haupt BJ. In-situ tower atmospheric measurements of carbon dioxide, methane and carbon monoxide mole fraction for the Indianapolis Flux (INFLUX) project, Indianapolis, IN, USA. Data set available on-line from The Pennsylvania State University Data Commons, 2017b; http://dx.doi.org/10.18113/D37G6P.

For further information, see http://sites.psu.edu/INFLUX.

Competing interests

The authors declare no competing interests.

Funding

This work is supported by the National Institute of Standards and Technology (Project # 70NANB10H245) and the National Oceanic and Atmospheric Administration (Award # NA13OAR4310076). T. Lauvaux was also supported by the French research program Make Our Planet Great Again (project CIUDAD).

Authors' contributions

Contributed to conception and design: NLM, TL, KJD, SJR, KRG, JCT
Contributed to acquisition of in-situ data: SJR, NLM, DKM
Contributed to modeling results: TL, AJD, JW, KRG, JL, GR
Contributed to analysis and interpretation of data: NLM, KJD, TL, JCT, NVB, SJR
Drafted article: NLM

Acknowledgements

The authors thank B. Haupt (The Pennsylvania State University) for assistance with scripting for data ingest and pre-processing and S. Miller (The Pennsylvania State University) for data quality assurance. Earth Networks supported the maintenance of INFLUX in-situ tower sites.

References

Bakwin PS, PP Tans, DF Hurst, C Zhao. Measurements of carbon dioxide on very tall towers: Results of the NOAA/CMDL program. Tellus 1998; 50B, 401–415.

Balashov NV, Davis KJ, Miles NL, Lauvaux T, Richardson SJ, Barkley ZR, and Bonin TA. Background heterogeneity and other uncertainties in estimating urban methane flux: Results from the Indianapolis Flux (INFLUX) Experiment. Atmos Chem Phys Discuss. 2019; doi.org/10.5194/acp-2019-48, in review.

Blasing TJ, Broniak CT, Marland G. The annual cycle of fossil-fuel carbon dioxide emissions in the United States. Tellus. 2005; 57B, 107–115.

Boon A, Broquet G, Clifford DJ, Chevallier F, Butterfield DM, Pison I, et al. Analysis of the potential of near-ground measurements of CO_2 and CH_4 in London, UK, for the monitoring of city-scale emissions using an atmospheric transport model. Atmos Chem Phys. 2016; doi:10.5194/acp-16-6735-2016.

Bréon FM, Broquet G, Puygrenier V, Chevallier F, Xueref-Remy I, Ramonet M, et al. An attempt at estimating Paris area CO_2 emissions from atmospheric concentration measurements. Atmos Chem Phys. 2015; doi:10.5194/acp-15-1707-2015.

Briber BM, Hutyra LR, Dunn AL, Raciti SM, Munger JW. Variations in atmospheric CO_2 mixing ratios across a Boston, MA urban to rural gradient. Land. 2013; doi:10.3390/land2030304.

Corbin KD, Denning AS, Lokupitiya EY, Schuh AE, Miles NL, Davis KJ, Richardson S, Baker, IT. Assessing the impact of crops on regional CO_2 fluxes and atmospheric concentrations. Tellus B. 2010; doi:10.1111/j.1600-0889.2010.00485.x

Davis KJ, Deng A, Lauvaux T, Miles NL, Richardson SJ, Sarmiento DP, et al. The Indianapolis Flux Experiment (INFLUX): A test-bed for anthropogenic greenhouse gas emission measurement and monitoring. Elem Sci Anth. 2017; doi.org/10.1525/elementa.188.

Deng A, Seaman NL, Hunter GK, Stauffer DR. Evaluation of inter-regional transport using the MM5/SCIPUFF system. J Appl Meteor. 2004; 43:1864–1886.

Deng A, Stauffer DR, Gaudet BJ, Dudhia J, Hacker J, Bruyere C, et al. Update on WRF-ARW end-to-end multi-scale FDDA system. 10th Annual WRF Users' Workshop, Boulder, CO. 2009. http://www2.mmm.ucar.edu/wrf/users/workshops/WS2009/abstracts/1-09.pdf. Accessed 17 Sept 2018.

Deng A, T Lauvaux, KJ Davis, BJ Gaudet, N Miles, S Richardson, et al. Toward reduced transport errors in a high resolution urban CO_2 inversion system. Elem Sci Anthropocene 2017; http://doi.org/10.1525/elementa.133.

Desert Research Institute, 2019. https://wrcc.dri.edu/cgi-bin/wea_windrose.pl?laKEYE. Accessed 15 November 2019.

Gervois S, de Noblet-Ducoudré N, Viovy N, Ciais P, Brisson N, Seguin B, et al. Including croplands in a global biosphere model: Methodology and evaluation at specific sites. Earth Int. 2004; 8:16.

Gurney KR, Razlivanov I, Song Y, Zhou Y, Benes B, Abdul-Massih M. Quantification of fossil fuel CO_2 emissions on the building/street scale for a large U.S. city. Environ Sci Technol. 2012; doi:10.1021/es3011282.

Gurney, K.R., J. Liang, R. Patarasuk, D. O'Keeffe, M. Hutchins, T. Lauvaux, J.C. Turnbull, P.B. Shepson. Reconciling the differences between a bottom-up and inverse-estimated FF CO_2 emissions estimate in a large US urban area, Elem Sci Anth. 2017; 5:44. doi:10.1525/elementa.137.

Gurney KR, Liang J, O'Keeffe D, Patarasuk R, Hutchins M, Huang J, et al. Comparison of global downscaled versus bottom-up fossil fuel CO_2 emissions at the urban scale in four U.S. urban areas. J Geophys Res Atmos. 2019; 124, 2823–2840.

Han W, Yang Z, Di L, Yue P. A geospatial web service approach for creating on-demand Cropland Data Layer thematic maps. Trans Amer Soc Agric Biol Eng. 2014; 57(1):239–247.

Hardiman BS, Wang JA, Hutyra LR, Gately CK, Getson JM, Friedl MA. Accounting for urban biogenic fluxes in regional carbon budgets. Science Total Environ. 2017; doi.org/10.1016/j.scitotenv.2017.03.028.

Heimburger AMF, Harvey RM, Shepson PB, Stirm BH, Gore C. Assessing the optimized precision of the aircraft mass balance method for measurement of urban greenhouse gas emission rates through averaging. Elem Sci Anth, 2017; doi.org/10.1525/elementa.134.

Hilton TW, Davis KJ, Keller K. Evaluating terrestrial CO_2 flux diagnoses and uncertainties from a simple land surface model and its residuals. Biogeosciences 2014; 11, 217–235.

Hollinger SE, Bernacchi CJ, Meyers TP. Carbon budget of mature no-till ecosystem in North Central Region of the United States. Agric For Meteor. 2005; 130: 59–69.

Jin S, Yang L, Danielson P, Homer C, Fry J, et al. 2013. A comprehensive change detection method for updating the National Land Cover Database to circa 2011. Remote Sens Environ 2013; 132: 159–175, doi.org/10.1016/j.rse.2013.01.012.

Kim Y, Moorcroft PR, Aleinov I, Puma MJ, Kiang NY. Variability of phenology and fluxes of water and carbon with observed and simulated soil moisture in the Ent Terrestrial Biosphere Model (ENT TBM version 1.0.1.0.0). Geosci Model Dev. 2015; doi.org/10.5194/gmd-8-3837-2015.

Kornei K. One fifth of Los Angeles's CO_2 rises from lawns and golf, Eos 2018; doi.org/10.1029/2018EO112149.

Lauvaux T, Schuh A, Uliasz M, Richardson S, Miles N, Andrews A, et al. Constraining the CO_2 budget of the corn belt: Exploring uncertainties from the assumptions in a mesoscale inverse system. Atmos Chem Phys. 2012; doi:10.5194/acp-12-337-2012.

Lauvaux T, Miles N, Richardson S, Deng AJ, Davis K, Stauffer D, et al. Urban emissions of CO_2 from Davos, Switzerland: The first real-time monitoring system using an atmospheric inversion technique. J Appl Meteor Climatol. 2013; doi.org/10.1175/JAMC-D-13-038.1.

Lauvaux T, Miles N, Deng A, Richardson S, Cambaliza MO, Davis KJ, et al. High resolution atmospheric inversion of urban CO_2 emissions during the dormant season of the Indianapolis Flux Experiment (INFLUX). J Geophys Res Atmos. 2016; doi:10.1002/2015JD024473.

Lauvaux, T., K.R. Gurney, N.L. Miles, K.J. Davis, S.J. Richardson, A. Deng, B.J. Nathan, T. Oda, J.A.Wang, L.R. Hutyra, and J.C.Turnbull: Policy-relevant assessment of urban greenhouse gas emissions, Environ Sci Tech. 2020; doi:10.1021/acs.est.0c00343.

Lokupitiya, E., Denning, S., Paustian, K., Baker, I., Schaefer, K., Verma, S., Meyers, T., Bernacchi, C. J., Suyker, A., and Fischer, M.: Incorporation of crop phenology in Simple Biosphere Model (SiBcrop) to improve land-atmosphere carbon exchanges from croplands, Biogeosciences, 6, 969-986, https://doi.org/10.5194/bg-6-969-2009, 2009.

McKain K, Wofsy SC, Nehrkorn T, Eluszkiewicz J, Ehleringer JR, Stephens B. Assessment of ground-based atmospheric observations for verification of greenhouse gas emissions from an urban region. Proc Nat Acad Sci 2012; doi:10.1073/pnas.1116645109.

Mahadevan P, Wofsy SC, Matross DM, Xiao X, Dunn AL, Lin JC, et al. A satellite-based biosphere parameterization for net ecosystem CO_2 exchange: Vegetation Photosynthesis and Respiration Model (VPRM). Global Biogeochem Cycles 2008; doi:10.1029/2006GB002735.

Miles NL, Richardson SJ, Davis KJ, Lauvaux T, Andrews AE, West TO, et al. Large amplitude spatial and temporal gradients in atmospheric boundary layer CO_2 mole fractions detected with a tower-based network in the U.S. Upper Midwest. J Geophys Res B. 2012; doi:10.1029/2011JG001781.

Miles NL, Richardson SJ, Lauvaux T, Davis KJ, Turnbull J, Karion A, et al. Quantification of urban atmospheric boundary layer greenhouse gas dry mole fraction enhancements: Results from the Indianapolis Flux Experiment (INFLUX). Elem Sci Anth, 2017a; doi.org/10.1525/elementa.127.

Miles NL, Richardson SJ, Davis KJ, Haupt BJ. In-situ tower atmospheric measurements of carbon dioxide, methane and carbon monoxide mole fraction for the Indianapolis Flux (INFLUX) project, Indianapolis, IN, USA. Data set available on-line from The Pennsylvania State University Data Commons, 2017b; doi.org/10.18113/D37G6P.

Mueller K, Yadav V, Lopez-Coto I, Karion A, Gourdji S, Martin C. et al. Siting background towers to characterize incoming air for urban greenhouse gas estimation: A case study in the Washington, DC/Baltimore area. J Geophys Res Atmos. 2018; doi.org/10.1002/ 2017JD027364.

Multi-Resolution Land Characteristics Consortium 2020. National Land Cover Database 2016 CONUS Land Cover. https://www.mrlc.gov/viewer/. Accessed 19 August 2020.

Nickless A, Rayner PJ, Engelbrecht F, Brunke E-G, Erni B, Scholes RJ. Estimates of CO_2 fluxes over the city of Cape Town, South Africa, through Bayesian inverse modelling. Atmos Chem Phys. 2018; doi.org/10.5194/acp-18-4765-2018.

Pal S, Davis KJ, Lauvaux T, Choi Y, DiGangi JP, et al. Greenhouse gas changes across summer frontal boundaries in the Eastern United States, J Geophys Res Atmos 2020; in review.

Richardson SJ, Miles NL, Davis KJ, Lauvaux T, Turnbull JC, Karion A, et al. CO_2, CO, and CH_4 surface in-situ measurement network in support of the Indianapolis Flux (INFLUX) Experiment. Elem Sci Anth. 2017; doi.org/10.1525/elementa.140.

Sargent M, Barrera Y, Nehrkorn T, Hutyra LR, Gately CK, Jones T, et al. Anthropogenic and biogenic CO_2 fluxes in the Boston urban area. Proc Natl Acad Sci U S A. 2018; doi.org/10.1073/pnas.1803715115.

Skamarock WC, JB Klemp. A time-split nonhydrostatic atmospheric model for weather research and forecasting applications. J Comput Phys. 2008; 227, 3465–3485.

Staufer J, Broquet G, Bréon F-M, Puygrenier V, Chevallier F, Xueref-Rémy I, et al. The first 1-year-long estimate of the Paris region fossil fuel CO_2 emissions based on atmospheric inversion. Atmos Chem Phys. 2016; doi:10.5194/acp-16-14703-2016.

Stauffer DR, Seaman NL. Multiscale Four-Dimensional Data Assimilation. J Appl Meteor. 1994; doi.org/10.1175/1520-0450(1994)033<0416:MFDDA>2.0.CO;2.

Turnbull J, Guenther D, Karion A, Sweeney C, Anderson E, Andrew A, et al. An integrated flask sample collection system for greenhouse gas measurements. Atmos Meas Tech. 2012; doi:10.5194/amt-5-2321-2012.

Turnbull JC, Karion A, Davis, KJ, Lauvaux T, Miles NL, Richardson SJ, et al. Synthesis of urban CO_2 emission estimates from multiple methods from the Indianapolis Flux Project (INFLUX). Environ Sci Techn. 2019; doi.org/10.1021/acs.est.8b05552.

Ueyama M, Ando T. Diurnal, weekly, seasonal and spatial variabilities in carbon dioxide flux in different urban landscapes in Sakai, Japan. Atmos Chem Phys. 2016; doi:10.5194/acp-16-14727-2016.

Uliasz M. Lagrangian particle modeling in mesoscale applications. in Environmental Modelling II. (Computational Mechanics Publications, Southampton, UK), 1994; No. 16282, pp. 71–102.

United States Census Bureau 2020. City and town population totals: 2010 – 2019 (dataset). https://www.census.gov/data/tables/time-series/demo/popest/2010s-total-cities-and-towns.html Accessed 19 August 2020.

United States Department of Agriculture, National Agricultural Statistics Service (USDA NASS 2019). https://nassgeodata.gmu.edu/CropScape/, Washington, DC. Accessed 30 May 2019.

Verhulst KR, Karion A, Kim J, Salameh PK, Keeling RF, Newman S, et al. Carbon dioxide and methane measurements from the Los Angeles Megacity Carbon Project - Part 1: Calibration, urban enhancements, and uncertainty estimates. Atmos Chem Phys. 2017; doi:10.5194/acp-17-8313-2017.

Wang W, Davis KJ, Yi C, Patton EG, Butler MP, Ricciuto DM, and Bakwin, PS. A note on top-down and bottom-up gradient functions over a forested site. Boundary-Layer Meteor. 2007; doi 10.1007/s10546-007-9162-0.

Whetstone JR. Advances in urban greenhouse gas flux quantification: The Indianapolis Flux Experiment (INFLUX). Elem Sci Anth. 2018; doi.org/10.1525/elementa.282.

Wu K, Lauvaux T, Davis KJ, Deng A, Lopez Coto I, Gurney KR, Patarasuk R. Joint inverse estimation of fossil fuel and biogenic CO_2 fluxes in an urban environment: An observing system simulation experiment to assess the impact of multiple uncertainties. Elem Sci Anth. 2018; 6(1):17, doi.org/10.1525/elementa.138.

Wu K. Joint estimation of fossil fuel and biogenic CO_2 fluxes in an urban environment, Ph.D. Dissertation 2020, The Pennsylvania State University, University Park, PA, USA.

Xueref-Remy I, Dieudonné E, Vuillemin C, Lopez M, Lac C, Schmidt M, et al. Diurnal, synoptic and seasonal variability of atmospheric CO_2 in the Paris megacity area. Atmos Chem Phys. 2018; doi.org/10.5194/acp-18-3335-2018.

Zeng N, Zhao F, Collatz GJ, Kalnay E, Salawitch RJ, West TO, Luis G. Agricultural Green Revolution as a driver of increasing atmospheric CO_2 seasonal amplitude. Nature 2014; doi.org/10.1038/nature13893.

Figures

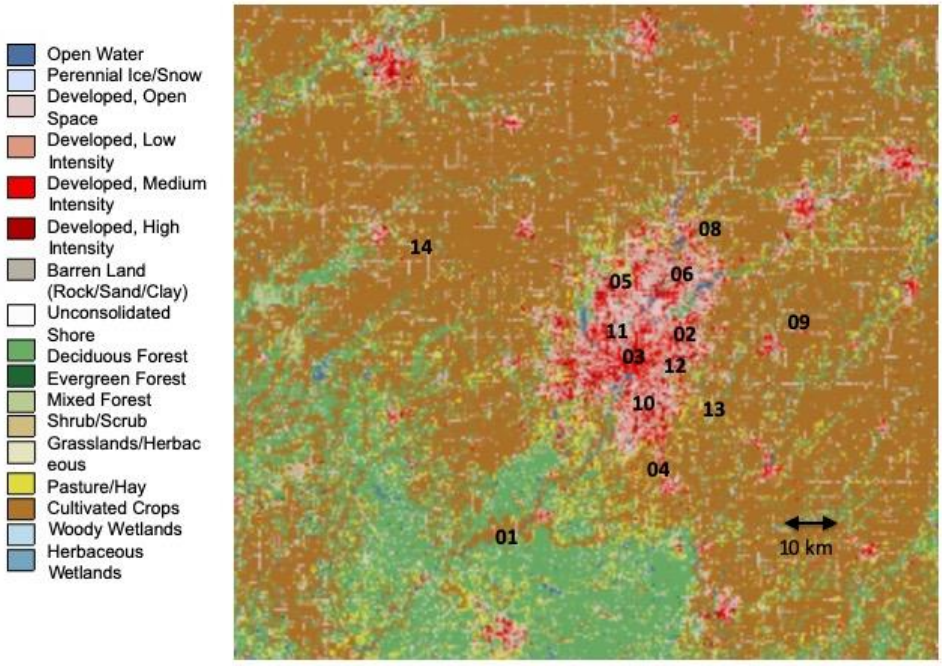

Figure 1. Landcover map of the Indianapolis, IN, region. The numbers 01–14 indicate tower site locations. Towers 05 and 12 were decommissioned in September 2015 and April 2013, respectively. Tower 14 was installed in April 2017 as an additional background site. (Multi-Resolution Land Characteristics Consortium 2020; Jin et al. 2013).

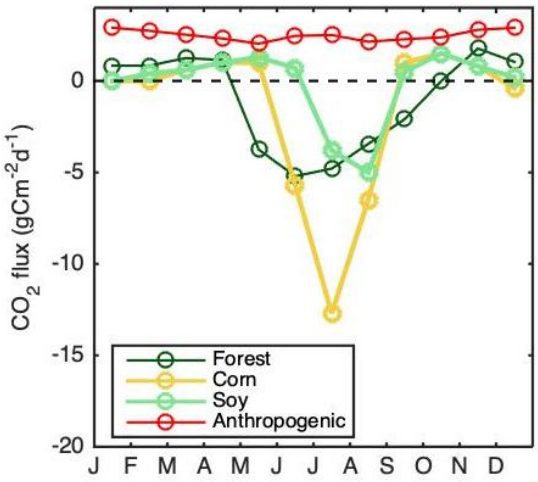

Figure 2. (a) Mean annual cycle of biological CO_2 fluxes (net ecosystem exchange; NEE) for a forest site (dark green), a corn site (yellow) and a soybean site (light green). The forest fluxes are the 5-year mean measured at the Morgan Monroe State Forest (Kim et al. 2015) and the corn and soybean fluxes are the 3-year mean measured in Bondville, Illinois (Hollinger et al. 2005). (b) Domain-averaged 31-day median (fossil fuel (Hestia) emissions as a function of time of year for 2014.

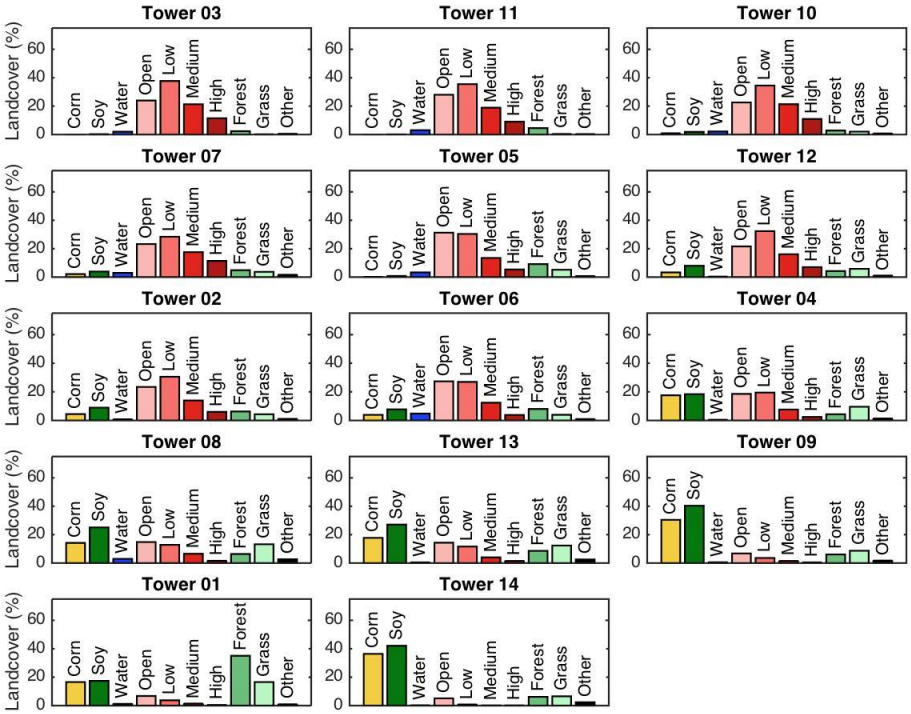

Figure 3. Percentage land cover types for a 10-km radius circle encompassing approximately 80 % of the footprint for each tower. (Han et al. 2014; United States Department of Agriculture National Agriculture Statistics Service 2019; https://nassgeodata.gmu.edu/CropScape/). https://nassgeodata.gmu.edu/CropScape/. The grass category also includes hay/pasture. Towers are ordered based on urban fraction (including open-, low-, medium-, and high-density developed areas). Towers 09, 01, and 14 are potential background towers.

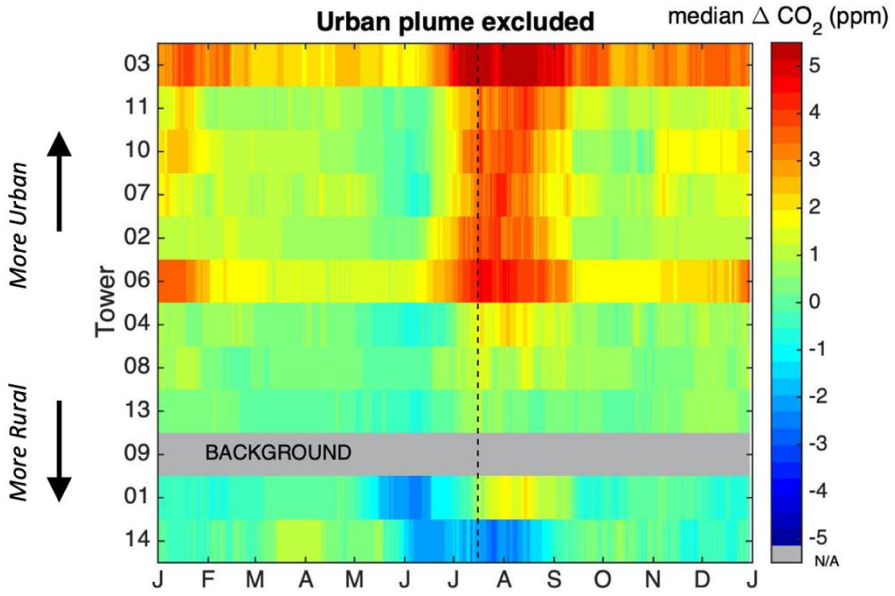

Figure 4. Composited 31-day running median afternoon-average CO_2 enhancements from Tower 09 for each of the towers, using data from January 2013 through December 2018. The towers are ordered by urban fraction (including high-, medium-, and low-density urban land cover, as discussed in Section 3.1. Tickmarks indicate the beginning of each time period. Data for which Tower 01 or Tower 09 was influenced by the urban plume were excluded from the analysis (WSW and NE). Dashed lines indicate July 15. Non-background towers deployed for less than 3 years are not shown (Towers 05 and 12). Tower 09 enhancement compared to Tower 09 is zero, by definition, but the row is included for consistency.

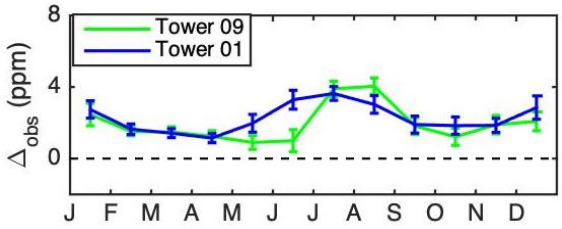

Figure 5. Observed CO_2 enhancement using Tower 09 (agricultural) as a background (green) and Tower 01 (forested) as a background (blue), composited over 2013 – 2018, and averaged over INFLUX urban towers. Wind directions for which either Tower 01 or Tower 09 are in the urban plume have been excluded. Only afternoon hours (1200 – 1700 LST) are included. Error bars indicate the standard error amongst the urban towers.

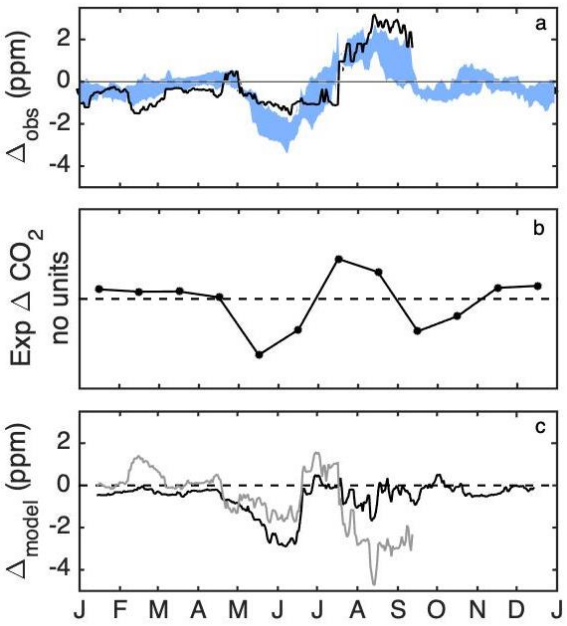

Figure 6. (a) 31-day running median CO_2 difference between Towers 09 and Tower 01 for 2014 (black line) and composited for 2013 – 2018 (shaded area), with the width of the shaded area indicating the standard deviation amongst years. Data for which either Tower 01 or Tower 09 were influenced by the urban plume were excluded from the analysis. (b) Predicted seasonal pattern of difference in CO_2 mole fraction (dimensionless, see Eq. 2) between Tower 01 and Tower 09, based on typical forest, corn and soy fluxes shown in Fig. 2a, and forest and agricultural land cover differences within 10 km of each site, between the two sites. (c) Forward modelled (using Hestia and VPRM) 31-day running median CO_2 difference (black) between Towers 09 and 01 for 2014. Difference between observed and modelled Tower 01 – Tower 09 difference is shown in gray.

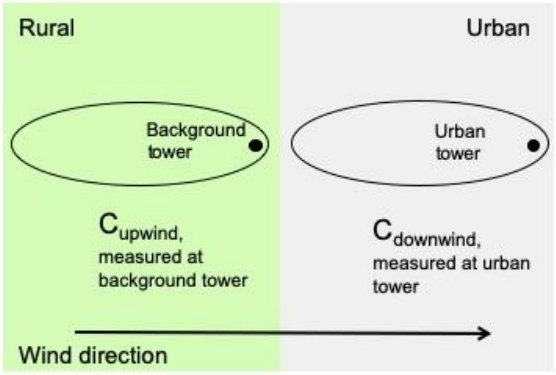

Figure 7. Schematic illustrating the "differential footprint" concept, as opposed to a simple box model. The green area indicates rural landcover surrounding the background tower and the gray area indicates urban landcover. The ellipses indicate the areas contributing the majority of the signal for each tower, since the influence decreases exponentially with distance from the tower. 80% of the influence for the INFLUX towers is within 10 km, on average, and for example, Towers 01 and 02 are separated by 43 km.

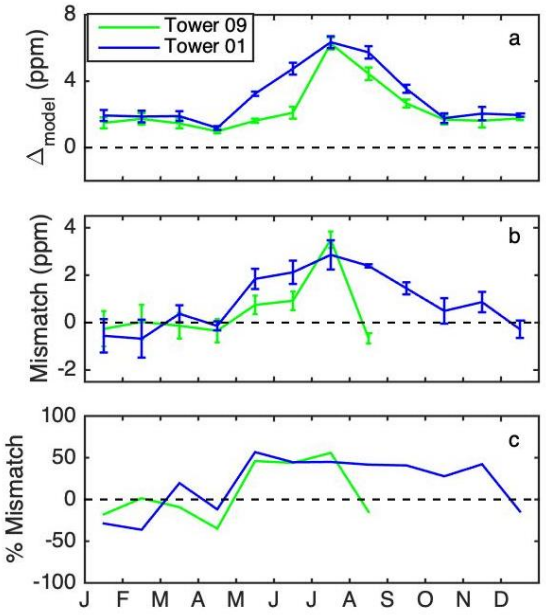

Figure 8. (a) Modelled CO_2 enhancement using Tower 09 (agricultural) as a background (green) and Tower 01 (forested) as a background (blue), averaged over INFLUX urban towers for 2014. Wind directions for which either Tower 01 or Tower 09 are in the urban plume have been excluded. Only afternoon hours (1200 – 1700 LST) are included. Error bars indicate the standard error amongst the urban towers. (b) Model-data mismatch. Note that there was an instrument failure at Tower 09 for September – December 2014. (c) Percent mismatch, i.e., model-data mismatch divided by the modelled CO_2 enhancement.

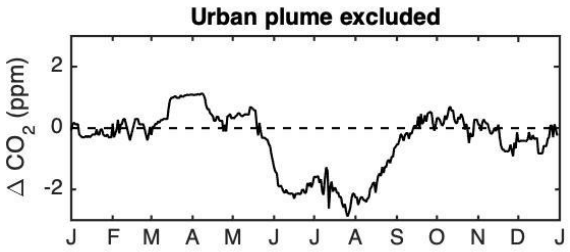

Figure 9. Composited 31-day running median CO_2 differences between Towers 09 and 14, both agricultural background towers. As for the previous results, data for which Tower 01 or Tower 09 was influenced by the urban plume were excluded from the analysis (WSW and NE). Tower 14 was not significantly affected by the urban plume.

Table 1. Measurement height(s) as of 2013 (with 2018 shown in parentheses if different) and predominant landcover type(s) at INFLUX towers. Additional tower details are listed in Miles et al. (2017). * Towers considered as background options (also italicized).

	Predominant landcover type(s)	Latitude (°N)	Longitude (°W)	Measurement height(s) (m AGL)
**Tower 01*	*Forest/agriculture*	*39.5805*	*86.4207*	*10/40/121*
Tower 02	Urban	39.7978	86.0183	10/40/136 (136)
Tower 03	Urban	39.7833	86.1652	10/20/40/54
Tower 04	Urban/agriculture	39.5925	86.1009	60
Tower 05	Urban	39.8947	86.2011	125
Tower 06	Urban	39.9201	86.0280	39
Tower 07	Urban	39.7739	86.2724	58
Tower 08	Agriculture/urban	40.0411	85.9734	41
**Tower 09*	*Agriculture*	*39.8627*	*85.7448*	*10/40/70/130 (130)*
Tower 10	Urban	39.7181	86.1436	40
Tower 11	Urban	39.8403	86.1763	130
Tower 12	Urban	39.7637	86.0403	40
Tower 13	Agriculture	39.7173	85.9417	87
**Tower 14*	*Agriculture*	*39.9971*	*86.7396*	*76*

Figure captions

Figure 1. Landcover map of the Indianapolis, IN, region. The numbers 01–14 indicate tower site locations. Towers 05 and 12 were decommissioned in September 2015 and April 2013, respectively. Tower 14 was installed in April 2017 as an additional background site. (Multi-Resolution Land Characteristics Consortium 2020; Jin et al. 2013).

Figure 2. (a) Mean annual cycle of biological CO_2 fluxes (net ecosystem exchange; NEE) for a forest site (dark green), a corn site (yellow) and a soybean site (light green). The forest fluxes are the 5-year mean measured at the Morgan Monroe State Forest (Kim et al. 2015) and the corn and soybean fluxes are the 3-year mean measured in Bondville, Illinois (Hollinger et al. 2005). (b) Domain-averaged 31-day median (fossil fuel (Hestia) emissions as a function of time of year for 2014.

Figure 3. Percentage land cover types for a 10-km radius circle encompassing approximately 80 % of the footprint for each tower. (Han et al. 2014; United States Department of Agriculture National Agriculture Statistics Service 2019; https://nassgeodata.gmu.edu/CropScape/). https://nassgeodata.gmu.edu/CropScape/. The grass category also includes hay/pasture. Towers are ordered based on urban fraction (including open-, low-, medium-, and high-density developed areas). Towers 09, 01, and 14 are potential background towers.

Figure 4. Composited 31-day running median afternoon-average CO_2 enhancements from Tower 09 for each of the towers, using data from January 2013 through December 2018. The towers are ordered by urban fraction (including high-, medium-, and low-density urban land cover, as discussed in Section 3.1. Tickmarks indicate the beginning of each time period. Data for which Tower 01 or Tower 09 was influenced by the urban plume were excluded from the analysis (WSW and NE). Dashed lines indicate July 15. Non-background towers deployed for less than 3 years are not shown (Towers 05 and 12). Tower 09 enhancement compared to Tower 09 is zero, by definition, but the row is included for consistency.

Figure 5. Observed CO_2 enhancement using Tower 09 (agricultural) as a background (green) and Tower 01 (forested) as a background (blue), composited over 2013 – 2018, and averaged over INFLUX urban towers. Wind directions for which either Tower 01 or Tower 09 are in the urban plume have been excluded. Only afternoon hours (1200 – 1700 LST) are included. Error bars indicate the standard error amongst the urban towers.

Figure 6. (a) 31-day running median CO_2 difference between Towers 09 and Tower 01 for 2014 (black line) and composited for 2013 – 2018 (shaded area), with the width of the shaded area indicating the standard deviation amongst years. Data for which either Tower 01 or Tower 09 were influenced by the urban plume were excluded from the analysis. (b) Predicted seasonal pattern of difference in CO_2 mole fraction (dimensionless, see Eq. 2) between Tower 01 and Tower 09, based on typical forest, corn and soy fluxes shown in Fig. 2a, and forest and agricultural land cover differences within 10 km of each site, between the two sites. (c) Forward modelled (using Hestia and VPRM) 31-day running median CO_2 difference (black) between Towers 09 and 01 for 2014. Difference between observed and modelled Tower 01 – Tower 09 difference is shown in gray.

Figure 7. Schematic illustrating the "differential footprint" concept, as opposed to a simple box model. The green area indicates rural landcover surrounding the background tower and the gray area indicates urban landcover. The ellipses indicate the areas contributing the majority of the signal for each tower, since the influence decreases exponentially with distance from the tower. 80% of the influence for the INFLUX towers is within 10 km, on average, and for example, Towers 01 and 02 are separated by 43 km.

Figure 8. (a) Modelled CO_2 enhancement using Tower 09 (agricultural) as a background (green) and Tower 01 (forested) as a background (blue), averaged over INFLUX urban towers for 2014. Wind directions for which either Tower 01 or Tower 09 are in the urban plume have been excluded. Only afternoon hours (1200 – 1700 LST) are included. Error bars indicate the standard error amongst the urban towers. (b) Model-data mismatch. Note that there was an instrument failure at Tower 09 for September – December 2014. (c) Percent mismatch, i.e., model-data mismatch divided by the modelled CO_2 enhancement.

Figure 9. Composited 31-day running median CO_2 differences between Towers 09 and 14, both agricultural background towers. As for the previous results, data for which Tower 01 or Tower 09 was influenced by the urban

plume were excluded from the analysis (WSW and NE). Tower 14 was not significantly affected by the urban plume.

Table caption

Table 1. Measurement height(s) as of 2013 (with 2018 shown in parentheses if different) and predominant landcover type(s) at INFLUX towers. Additional tower details are listed in Miles et al. (2017). * Towers considered as background options (also italicized).

Supplement

In this document, we discuss 1) differences in background site CO_2 as a function of time and wind direction, 2) enhancements compared to alternate backgrounds, 3) observed and modelled CO_2 enhancements, 3) corn production, and 4) tower height effects.

1) Differences in background site CO_2

1.1 Background CO_2 differences as a function of time

In general, the CO_2 time series for the three potential background towers (including all wind directions) was more variable in the summer months of July and August (Fig. S1a), due to the drawdown and respiration of the biosphere. Differences between the background sites were as large as 18 ppm (Fig. S1b). Examination of the diurnal cycles of the nine days in January – August 2018 with largest differences (Fig. S2) showed that the differences were attributable to the urban plume in most cases.

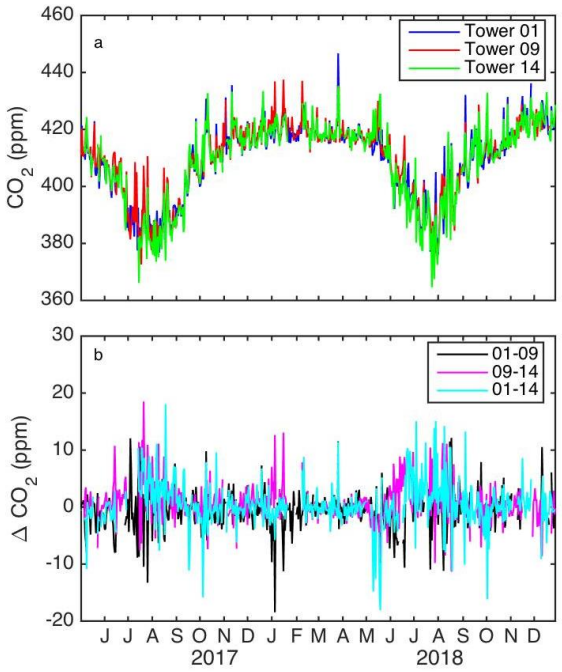

Figure S1. (a) Afternoon average CO_2 as a function of time for May 2017 – December 2018, for background towers (Towers 01, 09, and 14). (b) Afternoon average CO_2 difference between pairs of potential background towers, with all wind directions included. Tickmarks indicate the beginning of each month. Note that these plots include Tower 14 data for 26 April – 5 November 2017, a period with increased measurement uncertainty which are excluded from further analysis.

No evidence of differences in the timing of ABL growth between the towers was noted through examination of the hourly average values as a function of time of day for several examples of days with large inter-tower CO_2 differences (Fig. S2).

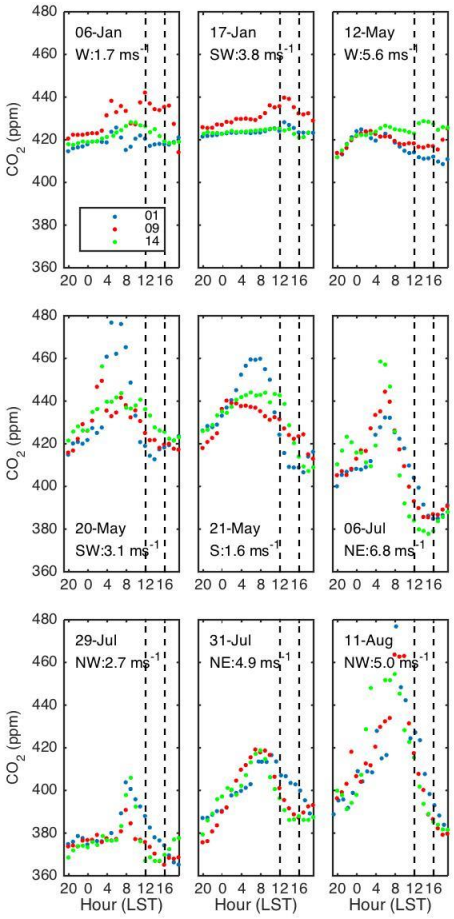

Figure S2. Hourly-averaged CO_2 for the six specific days with the largest deviations amongst the potential background towers for Tower 01 (blue), Tower 09 (red) and Tower 14 (green). Vertical dashed lines indicate 1200 and 1600 LST, the period over which the afternoon averages were determined. The date (in 2018) and afternoon-averaged wind direction and wind speed are indicated in each plot.

1.2 Background CO_2 differences as a function of wind direction

1.2.1 Tower 09 compared to Tower 01

During the dormant season (January/February), ABL CO_2 mole fraction differences between Towers 01 and 09 are dominated by the urban plume. The differences between background Towers 01 and 09 as function of afternoon average wind direction and speed are shown in Fig. S3a,c,e. For January and February for the years 2013–2018, the CO_2 measured at Tower 09 was 0.7 ppm higher than that at Tower 01, averaged over all wind directions. Examination of the differences as a function of wind direction revealed the effects of the city. The highest positive differences for these dormant season months were for wind directions from the NE, when Tower 01 was in the urban plume and measured 2.1–2.8 ppm CO_2 above that of Tower 09 (Fig. S3a). For the purposes of excluding the urban plume for subsequent analyses, we excluded wind directions between 20 – 65° for Tower 01, encompassing the large positive signals. When the wind direction was from the WSW, Tower 09 was in the urban plume, and the median Tower 09 CO_2 mole fraction was higher than that at Tower 01 by 1.7 ppm. We considered wind directions between 235 – 280° as those for which Tower 09 was affected by the urban plume. Although the differences for wind directions from the ESE and SSW were 1.6 and – 1.1 ppm, respectively, the wind directions were not such that either tower was downwind of the urban area. For the remaining wind directions, from the northwest and the southeast, the median differences were less than or equal to 0.3 ppm in magnitude or not significant compared to the standard error. We note that while Miles et al. (2017a) reported evidence of a CO_2 source to the SSE of Tower 01

during the period 1 January – 20 April 2013, we did not see such evidence when considering the increased statistics from multiple years of data.

During late spring (May/June), forest phenology causes the daytime ABL CO_2 mole fraction at Tower 01 to be persistently lower than the mole fractions observed at Tower 09 (Fig. S3c). Tower 01 CO_2 mole fractions were lower than Tower 09 by 1.7 ppm averaged over all wind directions. The largest median differences between Towers 09 and 01 occurred when the wind was broadly from the south, with median differences between 1.6 and 4.2 ppm. This pattern is consistent with seasonal timing differences in drawdown due to different land cover types at Tower 01 (largely forested) compared to Tower 09 (largely agricultural) and typical seasonal patterns in fluxes of those land cover types (Fig. 3). By May, leaf-out has typically occurred in the forested region south of Tower 01 (Kim et al. 2015), causing CO_2 drawdown at Tower 01 and larger magnitude negative differences compared to Tower 09. Agricultural drawdown is not maximized until July (Hollinger et al. 2005). When Tower 09 was in the urban plume, the differences were also large, up to 2.4 ppm. From other directions NNW through WSW, the magnitude of the median differences was small compared to the standard errors. The effect of the urban plume at Tower 01 (when wind directions were from the NE) were not apparent, unlike during the dormant season months.

During the peak growing season (July/August), the drawdown from the forest to the south of Tower 01 is not as apparent as the agricultural signal from the corn and soy surrounding Tower 09. The average difference over all wind directions switched in sign compared to May/June, and Tower 09 measured 1.4 ppm lower CO_2 than at Tower 01. For wind directions from the WSW when the urban plume affected Tower 09, the median Tower 09 CO_2 was higher than that at Tower 01 by up to 2.9 ppm for July/August (Fig. S3e), compared to 1.7 ppm higher from that direction in the dormant season. From wind directions broadly easterly, the median Tower 09 CO_2 was lower than Tower 01 by up to 4.5 ppm.

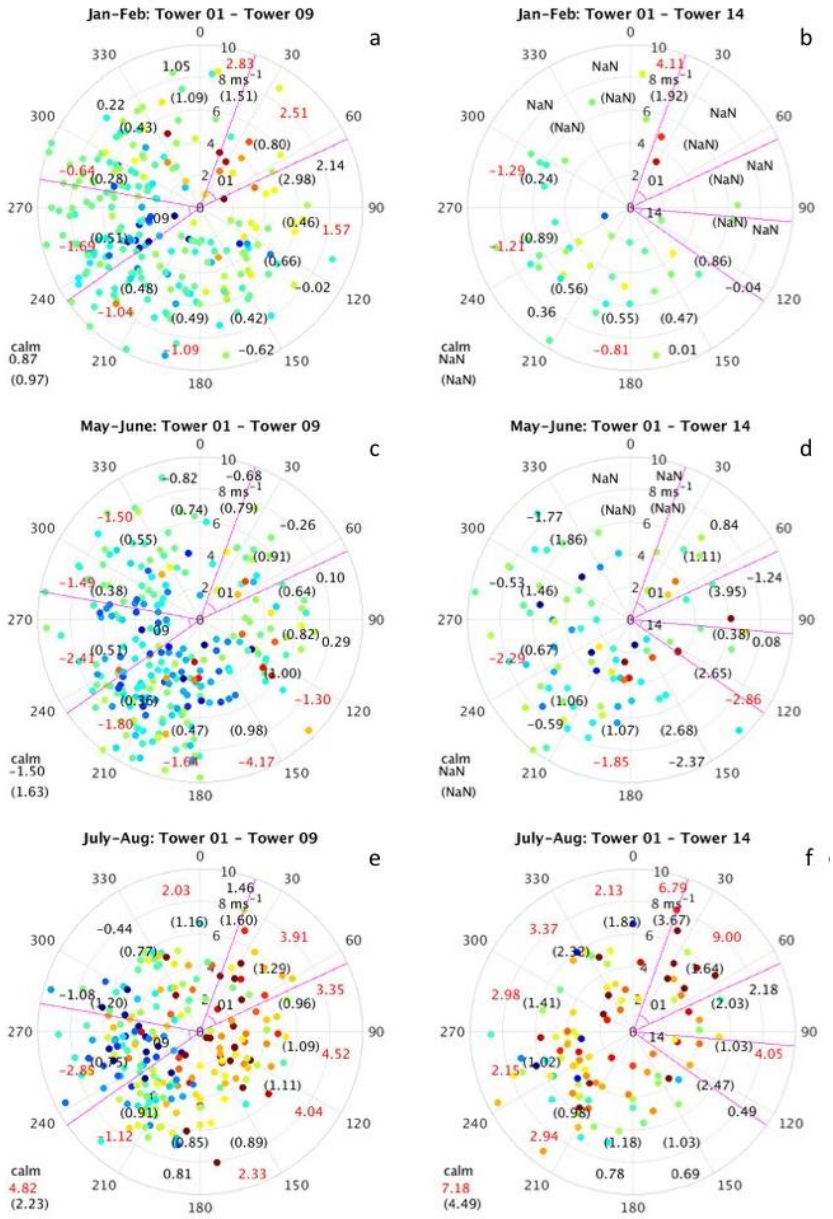

Figure S3. Afternoon-average CO_2 differences of Tower 09 from Tower 01 (a,c,e) and of Tower 14 from Tower 01 (b,d,f) as a function of wind direction (angle) and wind speed (radial distance) for various time periods. (a) For dormant season, January – February for the available years 2013 – 2018. The median CO_2 mole fraction within each wind direction range is indicated on the plots. The standard error for each wind direction range is indicated in parentheses. (b) For early growing season, May – June. (c) For late growing season, July – August. Magenta lines indicate the wind directions for which Towers 09 and 01, and Towers 14 and 01, respectively, were directly downwind of Indianapolis. Medians larger than the magnitude of the standard error by the measurement uncertainty (0.2 ppm) or larger are indicated by red numbers. Wind directions for which there are fewer than three days in the appropriate period are indicated by 'NaN'. For time periods with three or more afternoons with calm winds (<1.6 ms^{-1}), medians and standard errors are indicated in the lower left corner of each plot. Note that these plots include Tower 14 data for 26 April – 5 November 2017, a period with increased measurement uncertainty which are excluded from further analysis.

1.2.2 Tower 14 compared to Tower 01

While both Towers 01 and 09 were operational for the years 2013 – 2018, Tower 14 was deployed in 2017 as an additional background site. Thus there were fewer overall data points, as is particularly apparent when separated by wind direction (Fig. S3b,d,f).

On average over all wind directions, the median difference between Tower 14 and Tower 01 afternoon-average ABL CO_2 mole fraction was 0.0 ppm for the months of January and February, but the differences varied with wind direction according to the location of urban emissions. The CO_2 mole fractions observed at the two towers were not significantly different for most wind directions (Fig. S3b) during this period. The urban plume was not observed in the CO_2 measured at Tower 14 (wind directions from the southeast). Tower 14 is 44 km from the edge of Indianapolis. Tower 14 measured higher CO_2 with winds from the WNW and WSW by 1.2 – 1.3 ppm. The town of Crawfordsville is 13 km WNW of Tower 14. For the limited number of days for which the winds were from the NNE, Tower 01 was downwind of the city and measured 4.1 ppm higher CO_2 than Tower 14.

As was apparent in the comparison between Tower 01 and Tower 09, the afternoon CO_2 mole fraction at Tower 01 was lower than that measured at Tower 14 during May and June, coincident with drawdown from the forests south of Tower 01. Averaging over all wind directions, Tower 01 measured 1.1 ppm lower CO_2 during these months. As for Tower 09 during May/June, Tower 01 measured lower CO_2 than Tower 14 when wind directions were broadly southerly, specifically from SE to WSW, with median magnitude up to 2.9 ppm (Fig. S3d). When the wind directions were from remaining wind directions, the differences between the two towers was not significant compared to the standard error.

During the peak growing season months of July and August, crops (primarily corn and soy) played an important role in the CO_2 patterns observed at the background towers. Tower 14 measured 3.4 ppm lower CO_2 than Tower 01, with the difference for most wind directions being significant compared to the standard error (Fig. S3f). Larger differences are observed when the winds were aligned such that Tower 01 was downwind of the city, NNE and NE (up to 9.0 ppm). When the afternoon winds were calm, the median CO_2 at Tower 14 was 7.2 ppm lower than that of Tower 01.

2) Enhancements compared to alternate backgrounds

Large growing season enhancement is apparent for various alternate background considered, including the more Lagrangian approach of utilizing a wind-dependent background (Fig. S4). Some differences are, however, notable. When Tower 01 is used as the background, the growing season occurs earlier in the year (mid June rather than the beginning of August for Tower 09 as a background) (Fig. S4a). This shift is consistent with the timing of the typical fluxes of predominant land cover types surrounding these towers (Fig. 3). As has been described (Section 3.3.4), the growing season drawdown is stronger at Tower 14 compared to Tower 09 and the growing season enhancement at the urban sites is thus larger with this tower used as a background (Fig. S4b). Increased growing season enhancement is also apparent when using upwind towers as background (an Lagrangian approach, but not lagged in time) (Fig. S4d,e). We note that the enhancements shown in Fig. S4d,e cannot be directly compared to those in Fig. S4a-c because of differing wind directions.

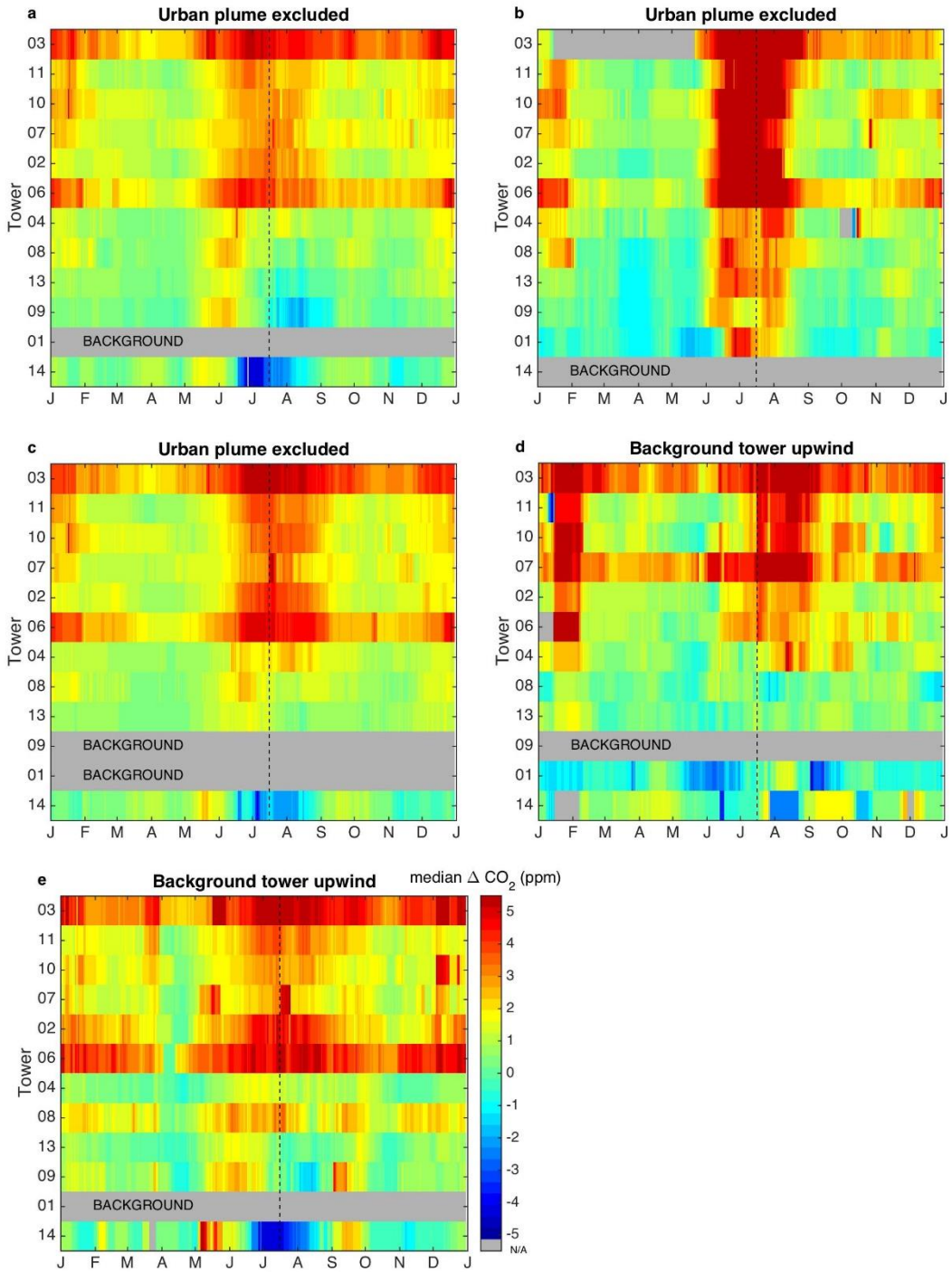

Figure S4. (a) Composited 31-day running median afternoon-average CO_2 enhancements from Tower 01 for each of the towers using data from January 2013 through December 2018. The towers are ordered by urban fraction (including high-, medium-, and low-density urban land cover, as discussed in Section 3.1. Tickmarks indicate the beginning of each time period. Data for which Tower 01 or Tower 09 was influenced by the urban plume were excluded from the analysis (i.e., days with SW or NE winds are excluded). Dashed lines indicate July 15. Non-background towers deployed for less than 3 years are not shown (Towers 05 and 12). (b) As in (a), but enhancements from Tower 14. (c) Composited CO_2 difference from a wind-direction dependent background (i.e., Tower 01 for wind directions between 180 – 360° and Tower 09 for 0 – 180°). To allow for comparison with a) and b), wind directions for which either background tower was affected by the urban plume are ignored. (d) Composited 31-day running median afternoon-average CO_2 difference from Tower 09 calculated over moving 31-day windows for each of the towers, using data from January 2013 through December 2018, only

when Tower 09 is upwind (55 – 100°). (e) As in (d), but composited CO_2 difference from Tower 01, when Tower 01 is upwind of the city (210 – 240°). The enhancements for (a) – (c) cannot be directly be compared with those for (d) and (e) because of differing wind directions.

3) U.S. corn production

The INFLUX region is on the edge of the U.S. corn belt, as shown in the map of U.S. corn production by county (Fig. S5).

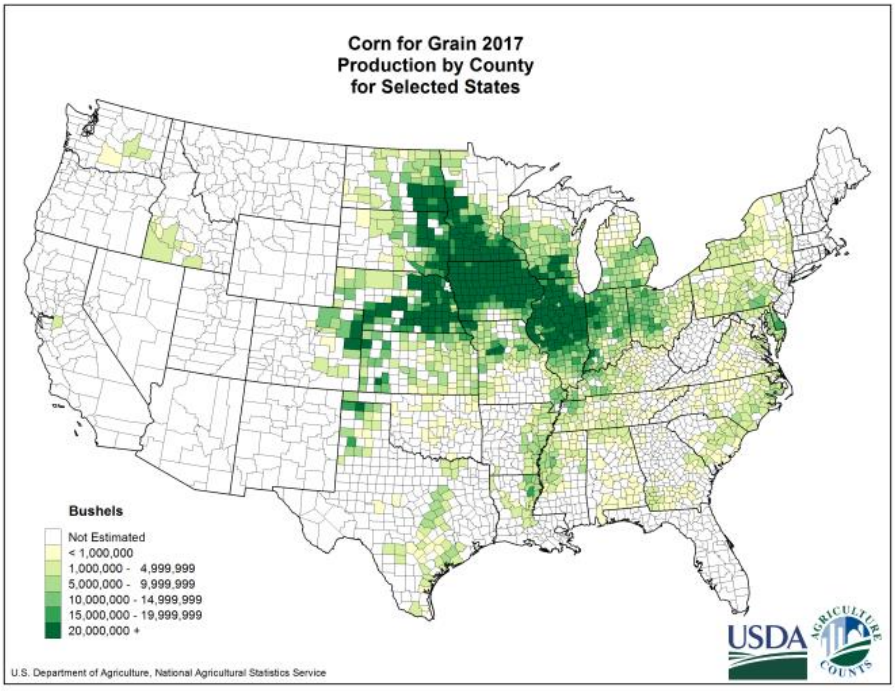

Figure S5. Corn production by county for 2017 (USDA NASS 2018).

4) Tower height effect on urban and rural CO_2 differences

Here we consider the effect on tower height on the results for urban and rural CO_2 differences. INFLUX towers 03, 10, 07, 06, 08, and 04 are 39 – 60 m AGL, whereas the remaining towers (including the background towers) are 87 m AGL or higher. The magnitude of the enhancement was certainly affected by the tower heights with the extent depending on the magnitude of the fluxes. For example, for a growing season period (1 June – 31 July 2013), the afternoon-only CO_2 measured at the top level (121 m AGL) at Tower 01 was 0.5 ppm greater than that measured at 40 m AGL (Fig. S6). Conversely dormant season CO_2 at Tower 01, with low fluxes at this background site, did not vary significantly with height. At Tower 03, the profiles were similar for growing and dormant seasons, and the CO_2 at the top level (54 m AGL) averaged 0.8 ppm above the 40 m AGL measurement, a large gradient consistent with large anthropogenic fluxes near that site.

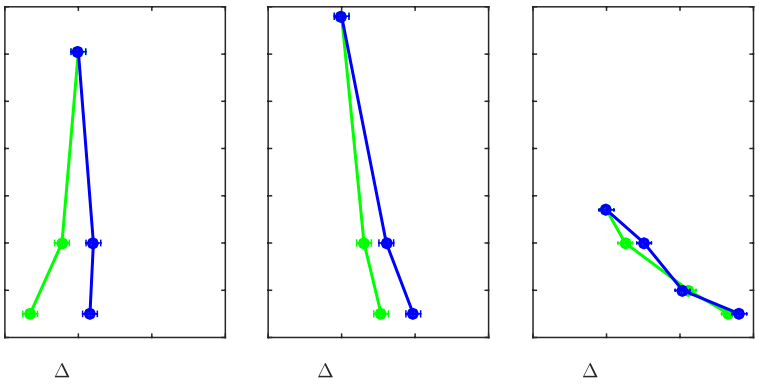

Figure S6. Composites of the difference between afternoon (1500–1600 LT) CO_2 measured at each level and that of the top level for a) Tower 01, b) Tower 02, and c) Tower 03. Green dots indicate the average for two months during the growing season (1 June – 31 July 2013) and blue dots, for two months during the dormant season (1 November – 31 December 2013). Bars indicate the accuracy of the CO_2 mole fraction measurements.

Despite the varying tower heights affected the enhancements, the predominant feature of large growing season enhancements is apparent regardless of tower height. The composited median CO_2 enhancements compared to Tower 01 are shown as a function of urban fraction and tower height in Fig. S7. For dormant season months of January/February (Fig. S7a), the demarcation between urban and rural towers is clear, despite differences in tower heights. Amongst the rural sites, there was a correlation between increasing CO_2 (primarily anthropogenic) and increasing urban fraction ($r^2 = 0.61$, $p = 0.12$ so 12 % probability of this correlation occurred by random chance). There was not a significant correlation between CO_2 and tower height ($r^2 = 0.16$, $p = 0.50$). Tower heights and urban fraction were weakly correlated ($r^2 = 0.49$, $p = 0.19$) for the rural sites, so completely deconvolving these effects was not possible.

The correlations between tower height, urban fraction, and median CO_2 enhancements were all low ($r^2 = 0.17 – 0.25$ and not significant) for the urban sites considered as a group. We also note that the median enhancements at Tower 03 (54 m AGL) during January/February were 4.3 ppm, whereas those at Tower 11 (130 m AGL) were 2.1 ppm, despite similar urban fractions. The urban land cover fraction does not include information on the spatial distribution of CO_2 sources and sinks or the predominant wind direction, and is not meant to be an exact predictor of CO_2 flux or CO_2 enhancements. The enhancements at Tower 03 are influenced by traffic emissions in the immediate vicinity of the tower.

For the peak growing season months of July/August, the separation between rural and urban sites was again apparent (Fig. S7b). If tower height were the dominant effect, we would expect agricultural towers with lower heights to measure lower CO_2 (more negative when compared to Tower 01), but this was not the case. Instead the CO_2 difference was dominated by urban fraction (associated with less biogenic signal).

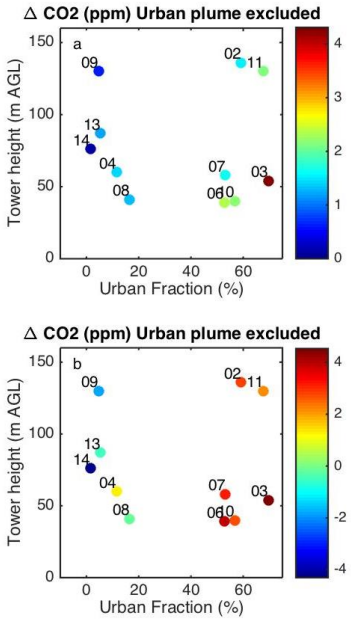

Figure S7. (a) Composited median (median for January/February) afternoon-average CO_2 enhancement from Tower 01, as a function of urban land cover fraction and tower height. Data for which Tower 01 or Tower 09 was influenced by the urban plume were excluded from the analysis (i.e., only days with NW or SE winds were included). 'Rural' towers with less than 17 % urban fraction include Towers 08, 04, 13, and 14, whereas the 'urban' towers had greater than 50 % urban fraction. (b) Same as (a), but for July/August. Note the differing scales for (a) and (b).